Single-copy expression of an amyotrophic lateral sclerosis-linked TDP-43 mutation (M337V) in BAC transgenic mice leads to altered stress granule dynamics and progressive motor dysfunction

David Gordon[1], Ruxandra Dafinca[1], Jakub Scaber[1], Javier Alegre-Abarrategui[2], Lucy Farrimond[1], Connor Scott[1], Daniel Biggs[3], Louisa Kent[1], Peter L. Oliver[2], Benjamin Davies[3], Olaf Ansorge[1], Richard Wade-Martins*[2] and Kevin Talbot[1]*

1. Nuffield Department of Clinical Neurosciences, University of Oxford, Oxford, UK

2. Department of Physiology, Anatomy and Genetics, University of Oxford, Oxford, UK 3. Wellcome Trust Centre for Human Genetics, Oxford, UK

*Address for correspondence:

Professor Kevin Talbot

Nuffield Department of Clinical Neurosciences, University of Oxford, West Wing, John Radcliffe Hospital, Oxford, OX3 9DU kevin.talbot@ndcn.ox.ac.uk

Professor Richard Wade-Martins

Department of Physiology, Anatomy and Genetics, University of Oxford, South Parks Rd, Oxford, OX1 3QX, UK Richard.wade-martins@dpag.ox.ac.uk

Abstract

Mutations in the gene encoding the RNA-binding protein TDP-43 cause amyotrophic lateral sclerosis (ALS), clinically and pathologically indistinguishable from the majority of 'sporadic' cases of ALS, establishing altered TDP-43 function and distribution as a primary mechanism of neurodegeneration. Transgenic mouse models in which TDP-43 is overexpressed only partially recapitulate the key cellular pathology of human ALS, but may also lead to non-specific toxicity. To avoid the potentially confounding effects of overexpression, and to maintain regulated spatio-temporal and cell-specific expression, we generated mice in which an 80kb genomic fragment containing the intact human TDP-43 locus (either TDP-43^{WT} or TDP-43^{M337V}) and its regulatory regions was integrated into the *Rosa26 (Gt(ROSA26)Sor)* locus in a single copy. At 3 months of age, TDP-43^{M337V} mice are phenotypically normal but by around 6 months develop progressive motor function deficits associated with loss of neuromuscular junction integrity, leading to a reduced lifespan. RNA sequencing shows that widespread mis-splicing is absent prior to the development of a motor phenotype, though differential expression analysis reveals a distinct transcriptional profile in pre-symptomatic TDP-43^{M337V} spinal cords. Despite the presence of clear motor abnormalities, there was no evidence of TDP-43 cytoplasmic aggregation *in vivo* at any timepoint. In primary embryonic spinal motor neurons and in embryonic stem cell (ESC)derived motor neurons, mutant TDP-43 undergoes cytoplasmic mislocalisation, and is associated with altered stress granule assembly and dynamics. Overall, this mouse model provides evidence that ALS may arise through acquired TDP-43 toxicity associated with defective stress granule function. The normal phenotype until 6 months of age can facilitate the study of early pathways underlying ALS.

Introduction

Amyotrophic lateral sclerosis (ALS) is a late onset, rapidly progressive, neurodegenerative disease characterised by degeneration of upper and lower motor neurons leading to weakness, spasticity, paralysis and ultimately death from respiratory failure with a median survival from symptom onset of 30 months (Rowland and Shneider, 2001; Talbot, 2009). The majority of ALS cases are not associated with a clear family history (so-called 'sporadic ALS'), and are presumed to be caused by a combination of complex genetic susceptibility, age-dependent stochastic changes in cellular homeostasis, and as yet unidentified environmental factors, in a 'multistep' model (Al-Chalabi *et al.*, 2014). Approximately 10% of ALS cases are familial (FALS), mostly caused by a single mutation inherited in an autosomal dominant pattern (Da Cruz and Cleveland, 2011). Mutations in the same genes responsible for FALS are found in a significant minority of clinically indistinguishable SALS cases, suggesting that genetic factors are likely to be relevant to most cases of ALS and the distinction between familial and sporadic ALS is not absolute (Talbot, 2011).

The common neuropathological marker in over 95% of cases of both sporadic and familial ALS is the redistribution of the protein TDP-43 (43-kDa transactive response DNA-binding protein) from a predominantly nuclear localisation to form insoluble ubiquitinated aggregates in the cytoplasm of affected motor neurons (Arai *et al.*, 2006; Neumann *et al.*, 2006). TDP-43 is a DNA/RNA-binding protein containing an N-terminal domain, two RNA-recognition motifs and a glycine-rich C-terminal domain thought to be important for mediating proteinprotein and protein-RNA interactions, especially with heterogeneous nuclear ribonucleoproteins (hnRNPs). A wide variety of physiological roles for TDP-43 have been identified, including in transcription, translation, splicing, nucleocytoplasmic shuttling, transport for local translation, and in stress granule assembly (Lagier-Tourenne *et al.*, 2010; Buratti and Baralle, 2012). More than 50 mutations in the associated gene, *TARDBP*, have

been identified in SALS and FALS patients, with the majority affecting residues clustered in the glycine-rich C-terminal region and predicted to affect RNA-protein or protein-protein interactions (Gitcho *et al.*, 2008; Kabashi *et al.*, 2008; Sreedharan *et al.*, 2008; Van Deerlin *et al.*, 2008). These mutations directly implicate abnormal TDP-43 dysfunction in the mechanism of ALS. However, it is currently unclear whether TDP-43-mediated neurodegeneration is driven by depletion of TDP-43 from the nucleus and loss of its constitutive splicing function, by an acquired nuclear or cytoplasmic toxicity, or a combination of factors (Neumann *et al.*, 2006; Van Deerlin *et al.*, 2008). The presence of ubiquitinated protein aggregates containing TDP-43 is a neuropathological marker of ALS, but aggregation itself may not be an intrinsic pathogenic mechanism or a necessary condition for the development of ALS. A significant proportion of cases of frontotemporal dementia (FTD) are part of a clinical, genetic and neuropathological spectrum with ALS, indicating common molecular pathways mediated by TDP-43 mislocalisation (Neumann *et al.*, 2006; Cairns *et al.*, 2007; Hasegawa *et al.*, 2008). Models of TDP-43-associated ALS are therefore likely to also provide insights into FTD, the second commonest cause of dementia (Janssens and Van Broeckhoven, 2013).

A range of mouse models expressing wild-type or mutant forms of TDP-43 have been generated, based on either cDNA-derived overexpression of the transgene by ubiquitous or neuronally expressed promoters or randomly integrated genomic constructs (Wegorzewska *et al.*, 2009; Shan *et al.*, 2010; Stallings *et al.*, 2010; Tsai *et al.*, 2010; Wils *et al.*, 2010; Xu *et al.*, 2010; Xu *et al.*, 2011). TDP-43 models have recapitulated some features of TDP-43associated ALS, but the highly variable disease phenotypes seen in these mice may reflect pathways not relevant to human ALS, including non-specific toxicity from TDP-43 overexpression. Hemizygous PrP-driven TDP-43^{M337V} mice, with lower levels of TDP-43

expression, have previously been observed to display motor deficits in conjunction with TDP-43 cytoplasmic mislocalisation (Wang *et al.*, 2017).

Bacterial artificial chromosome (BAC)-based transgenic mouse lines express genes from genomic DNA inserts with their native promoter under the control of flanking enhancer and silencer elements, and preserve expression of multiple splice variants (Wade-Martins *et al.*, 2001). Conventionally, BAC transgenesis is based on random integration, and consequently copy number variations and position effects can still complicate comparative analyses between mutant and wild-type overexpression. Here, we adopt a new strategy, combining the advantages of BAC-based transgenic constructs with a targeted transgenic approach, to allow a single copy of each BAC construct to be integrated into a defined neutral position within the genome. We have generated transgenic mice in which a single copy BAC construct containing human TDP-43, either wild-type (WT) or with an ALS-associated TDP-43 mutation (M337V) has been specifically inserted into the mouse *Rosa26 (Gt(ROSA26)Sor* locus. In contrast to human TDP-43^{WT}, expression of TDP-43^{M337V} leads to progressive motor impairment and loss of neuromuscular integrity from 6 months, and reduced survival, in a temporal sequence which will facilitate the exploration of the early steps in ALS pathogenesis. Primary motor neurons expressing mutant TDP-43 show a mutation specific defect in stress granule dynamics, and RNA sequencing in mouse spinal cord shows that a general alteration in splicing is absent before disease initiation. This model provides evidence that TDP-43 dysfunction leading to motor neuron degeneration is most likely to be due to an acquired toxic property of the protein rather than loss or alteration of its function in splicing.

Materials & methods

Human genomic TDP-43 vector construction

The generation of the TDP-43-BAC constructs has been described previously (Mutihac *et al.*, 2015). The pBACe3.6 plasmid RP11-829B14 containing the full-length genomic locus of *TARDBP* (202.43 kb) was obtained from the BACPAC Resources Centre at Children's Hospital Oakland Research Institute, Oakland, CA. The 47.5 kb *TARDBP* genomic locus, including a 30 kb regulatory upstream region and a 5 kb downstream region, was subcloned into a 9.5 kb pCYPAC2 plasmid using a Red/ET-based strategy for homologous recombination (Alegre-Abarrategui *et al.*, 2009). Briefly, the pCYPAC2 plasmid was amplified with 4 primers for the addition of 110 bp homology arms to the upstream and downstream regions of interest in the *TARDBP* genomic locus, and correct subcloning was assessed by restriction digests and PCR. The Ypet reporter gene was inserted by two rounds of homologous recombination, which involved a two-step process based on the dual resistance/sensitivity cassette pRpsl-Chl. Conventional site-directed mutagenesis was used to insert the M337V missense mutation (bp1009, A>G) in exon 6 using Stratagene Pfu Turbo polymerase. The mutation was engineered in a cDNA TARDBP plasmid and the entire exon 6 carrying the correct mutation was exchanged with exon 6 from the TDP-43 BAC.

Animal work

The generation and phenotyping of the TDP-43^{M337V} and TDP-43^{WT} mouse models was carried out in accordance with Animal [Scientific Procedures] Act 1986, with procedures reviewed by the clinical medicine animal care and ethical review body (AWERB), and conducted under project licenses PPL30/2966 and PPL 30/3353. All applicable international, national, and institutional guidelines, including ARRIVE guidelines, for the care and use of animals were followed. Animals were housed in specific pathogen free conditions, with the only reported positives on health screening over the entire time course of these studies being for Helicobacter hepaticus and Entamoeba spp. All animals were housed in social groups of balanced genotype, age and sex, with wildtype littermates as controls. All cages were of

mixed genotype, with 3-5 mice per cage provided with food and water ad-libitum and, maintained on a 12h light: 12h dark cycle (150–200 lux cool white LED light, measured at the cage floor). Phenotyping experiments were blinded and randomised, with mice identified only by codes and earclip number until all testing was completed. All environmental changes were applied to all animals and no animals were excluded from the study. No single housed mice were included in studies.

Mouse generation

The BAC vectors were retrofitted via the loxP site within the backbone of pCYPAC2 with a vector containing PhiC31 integrase attB sites and a promoterless Neomycin selection cassette. The vectors were then targeted to the *Rosa26 (Gt(ROSA26)Sor)* locus in embryonic stem cells (ESCs) by *Phi*C31 integrase-mediated cassette exchange into IDG26.10-3 ESCs, which harbour an PhiC31 attB flanked hygromycin cassette, pre-integrated at the Rosa26 (Gt(ROSA26)Sor) locus (Chen *et al.,* 2011). G418 resistant ESCs were screened by PCR screening and immunoblotting to 1) confirm correct exchange (integration) at the 5' and 3' end using the two primer combination ExPGK3 (5'-CACGCTTCAAAAGCGCACGTCTG-3') and ExNeo2 (5'-GTTGTGCCCAGTCATAGCCGAATAG-3'); allBac-F1 (5'-TTAGGTCCCTCGACCTGCAGG-3') and Rosa3HR-R (5'-CGGGAGAAATGGATATGAAGTACTGGGC-3'), respectively and 2) to ensure all regions of the human genomic BAC were present. Candidate TDP-43^{WT} and TDP-43^{M337V} ESCs were injected into C57BL/6 blastocysts and the resulting chimeric embryos transferred to recipient pseudopregnant females. Chimeric male founder mice (F1) were subsequently crossed with C57BL/6J female mice to generate two isogenic human TDP-43 transgenic lines, differing only by the presence or absence of the M337V mutation. Mice were again screened by PCR using a battery of primers to confirm correct integration and presence of the BAC vector regions. Retention of the TDP-43^{M337V} mutation in exon 6 was confirmed by

sequencing DNA from ESCs and subsequent chimeric founders. Founder mice were backcrossed to C57BL/6J for a minimum of 3 generations and homozygous and heterozygous transgenic lines were established. To minimise the effects of genetic background, all experimental control animals were age-matched littermates. These TDP-43^{M337V} BAC mice are available from The Jackson Laboratory as strain JAX#029266, https://www.jax.org/strain/029266.

RNA extraction

20 mg of cerebral cortex or lumbar spinal cord was homogenised in 500 µl of Trizol reagent (Invitrogen) with a disposable, motorised pestle (Sigma). After resting for 5 min, 300 µl of chloroform was added and the mixture shaken to thoroughly mix the organic and aqueous phases. The suspension was rested on ice for 5 min, and then centrifuged at 12,000g for 15 min at 4□C. The aqueous layer containing total RNA was removed and 1 volume of 70% ethanol added. Total RNA was further purified using the RNeasy Mini kit as per the manufacturer's instructions with on-column DNase digestion (Qiagen).

Protein extraction and Immunoblotting

20 mg of cerebral cortex or lumbar spinal cord, or cell were washed with phosphate-buffered saline (PBS). Protein was extracted in RIPA buffer (Pierce; (0.5% sodium deoxycholate, 0.1% SDS, 1% NP-40) containing 1% Halt protease inhibitor cocktail (Thermo Scientific). Cells were scraped from wells, while tissue was homogenised using a disposable, motorised pestle. The resulting protein suspension was centrifuged at 16000 × *g* for 15 min at 4^{o}C. The supernatant (soluble fraction) was retained. The remaining insoluble protein pellet was resuspended in urea buffer (7 M urea, 2 M thiourea and 4% CHAPS in 30 mM Tris buffer, pH8.5) and homogenised with a disposable, motorised pestle followed by centrifugation at

16000 × *g* for 30 min at room temperature. The supernatant comprising the insoluble protein fraction was collected. Nuclear and cytoplasmic fractionation was carried out using the NE-PER nuclear and cytoplasmic extraction kit (Pierce) according to manufacturer's instructions. Protein concentration was quantified using the BCA protein assay kit (Pierce) according to the manufacturer's instructions. Protein was boiled in Laemmli buffer for 5 min at 95 °C and 5–10 μg were loaded on gels. For Western blot analysis, lysates were resolved on a SDSPAGE (10% or 12% Tris–glycine gel) using a Mini-Protean Tetra electrophoresis system (BioRad) under constant voltage (100 V for 1 h) and transferred to a methanol activated polyvinylidene difluoride membrane (Immobilon-P, PVDF) using the Mini Trans-blot cell system under constant voltage (25 V for 2 h). Blots were blocked in a blocking buffer (PBS, 1% Tween-20, 5% skimmed milk) for 1 h at room temperature and then incubated in PBS, 1% Tween-20 and 1% milk with primary antibodies overnight at 4°C. Primary antibodies used were rabbit anti-*pan*TDP-43 (ProteinTech, Cat. number 10782-2-AP, 1:2000) and rabbit anti-actin (Sigma, Cat. number A2066, 1:2000). Nuclear fractions were identified with mouse anti-histone H3 (Abcam, Cat. number ab24834, 1:1000), while cytoplasmic fractions were identified using mouse ant-GAPDH (Abcam, Cat. number ab9484; 1:500). Horseradish peroxidase (HRP)-conjugated anti-mouse IgG (BioRad, 1:10000) or anti-rabbit IgG (BioRad, 1:10000) were used as secondary antibodies. Signal was visualized using the ECL or ECL Plus detection system (Amersham Pharmacia Biotech). The integrated optical density of each band was measured in ImageJ or ImageStudio and expression normalized to actin levels in the same samples for comparative expression assessment.

Polymerase chain reaction

Amplification of DNA was performed using MegaMix-Blue master mix (Clent Life science) according to manufacturer's instructions. Primers used for mouse genotyping: *Rosa26* sense: 5'- AAAGTCGCTCTGAGTTGTTAT-3'; *Rosa26* antisense: 5'-

GGAGCGGGAGAAATGGATATG-3'; Ypet sense: 5'- AAGTCTTCTGGCTGGGGAAT-3'; Ypet antisense: 5'- GGTCTTGTAGTTGCCGTCGT-3'. Mouse interleukin2 primers were used as positive controls for DNA. Mouse interleukin2 sense: 5'-CTAGGCCACAGAATTGAAAGATCT-3'; Mouse interleukin2 antisense: 5'-GTAGGTGGAAATTCTAGCATCATCC-3'. Sequencing of the mutation-containing region from exon 6 of the BAC from TDP-43^{M337V} ESC or mouse genomic DNA confirmed the presence of the mutation (A>G) compared to TDP-43^{WT}. Human TDP-43 exon 6.1 sense: 5'-TGAATCAGTGGTTTAATCTTCTTTG-3'; human TDP-43 exon 6.1 antisense: 5'TGCTGCACCAGAATTAGAGC-3'; human TDP-43 exon 6.1 sequencing sense: 5'GGATGAACTTTGGTGCGTTC-3'; human TDP-43 exon 6.1 sequencing antisense 5'TGGCTCCCTCTGCATGTTGC-3'. **cDNA generation and qRT-PCR** cDNA was generated using the High-Capacity cDNA Reverse Transcription Kit (ThermoFisher) according to manufacturer's instructions. qRT-PCR was carried out using LightCycler® 480 SYBR Green I Master mix (Roche) on a Lightcycler 480 instrument II (Roche). CNS samples were tested in triplicate using the following primers, previously tested for linearity: Human TDP-43 sense: 5'-GTGTGGGCTTCGCTACAGG-3'; human TDP-43 antisense 5'-CAACATACACCAGATTTCCCCAG-3'; mouse TDP-43 sense 5'-ATGAGAACGATGAACCCATTGAA-3'; mouse TDP-43 antisense 5'-TGAGACACGGGATTCCGGTAG-3'; mouse 18S sense 5'GAGGCCCTGTAATTGGAATGAG-3'; mouse 18S antisense 5'GCAGCAACTTTAATATACGCTATTGG-3'; mouse GAPDH sense 5'GGCTGCCCAGAACATCATCCCT-3'; mouse GAPDH antisense 5'-ATGCCTGCTTCACCACCTTCTTG-3'; mouse neuron specific enolase (NSE) sense 5'-AGGTGGATCTCTATACTGCCAAA-3'; mouse NSE antisense 5'-

GTCCCCATCCCTTAGTTCCAG-3'. Relative change in gene expression was analysed using the $2^{-\Delta\Delta CT}$ method (Livak and Schmittgen, 2001).

Neuropathology

Immunohistochemistry (IHC) assays were performed on the Ventana Discovery Ultra automated immunostainer (Ventana Medical Systems, Tucson, AZ). On-board baking and deparaffinization were performed for 24 min at 37°C, or 24 min at 60°C for Iba1 immunohistochemistry. Antigen retrieval was done on-board at 95°C for 64 minutes with CC1 reagent, which is an EDTA-based proprietary Ventana solution (pH 8.0–8.5). Rabbit anti-TDP-43 (ProteinTech, Cat. number 10782-2-AP, 1:15000) was applied and incubated for 44 minutes at 37°C. Mouse anti-phospho TDP-43 (Cosmo Bio, Cat. number TIP-PTD-M01, 1 :30000) was applied and incubated for 2 hours at 37°C. An anti-IgG1 + IgG2a + IgG3 rabbit monoclonal antibody was used to minimise species cross-reactivity, and was applied for 28 minutes at 37°C. Mouse anti-(human specific) TDP-43 (Proteintech, Cat. number 60019-2-Ig, 1:5000) was applied and incubated for 44 minutes at 37°C. An anti-IgG1 + IgG2a + IgG3 rabbit monoclonal antibody was used to minimise species cross-reactivity, this was applied for 28 minutes for 37°C. Rabbit anti-Iba1 (WAKO, Cat. number 019-19741, 1:5000) was applied and incubated for 32 minutes at 37°C. Slides were developed using antirabbit HQ (Ventana, Cat. number 760–4815) and anti-HQ HRP (Ventana, Cat. number 7604820) and were detected using ChromoMap DAB (Ventana, Cat. number 760–159). Sections from n=3 mice from each line were analysed semi-quantitatively and blinded to genotype.

Motor function testing

Accelerating rotarod

A minimum of 12 mice per sex per genotype were analysed for motor performance (Table 1). Cohorts of age-matched, sex-matched transgenic mice and littermate non-transgenic (NTg) controls were tested for time to fall from the accelerating rotarod. Mice were given a training session 5-7 days before testing, in which mice were acclimatised to staying on the rotarod. All mice were stable on the rotarod for at least 5 sec before beginning the programmed run of 4-40 rpm. Animals were tested 3 times each day between the hours or 12-5 pm, over 3 separate days, at each testing age (3, 6, 9, 12 and 18 months) with an average of 9 replicates used for analysis. Mice were rested for at least 1 hr between trials. If a mouse held onto the rod for 3 revolutions, rather than running, then that counted as a fall for that mouse. The time at which mice fell from the rotarod was recorded, up to a maximum time of 300s.

Grip strength

The four-limb hanging wire test is a test of muscle strength using all four limbs (sustained tension in the limb musculature). All mice were tested between the hours or 12-5 pm, and weighed before the start of the trials. Mice were placed on the centre of a wire mesh screen (43 cm square of wire mesh consisting of 12 mm squares of 1 mm diameter wire). The timer was started and the screen inverted over 2s with the head of the mouse inverting first, with the screen held 35-40 cm above a horizontal surface. Mice were tested 3 times each day at each testing stage (3, 6, 9, 12 and 18 months), over 2 separate days with an average of 6 replicates used for analysis. The time at which mice fell from the wire mesh was recorded, up to a maximum time of 120s. Mice were rested for at least 15 min in between trials. To correct for any effect of weight on grip strength, animals were weighed on the day of testing, and the holding impulse (weight × hang time) calculated. There was no significant effect of weight on the progressive decline of grip strength observed in the TDP-43^{M337V} mice over the timecourse of the experiment (Supp. Fig. 2).

Open Field

Open field testing assesses novel environment exploration and general locomotor activity. Mice were given 20 min in the locomotor activity (LMA) box two days prior to testing. On the day of testing, mice were acclimatised to the room for 15 min prior to testing and allowed 10 minutes to acclimatise to the box prior to recording. Activity was recorded for 20 minutes, once per day for 2 days at approximately the same time each day. Activity was recorded using the AMLogger with activity monitor software AM1053 (Linton Instrumentation, England). During recording the tester kept activity to a minimum, and remained out of sight of the LMA boxes. LMA boxes were rinsed and cleaned between trials.

Muscle preparation and NMJ immunocytochemistry

Mice were sacrificed, lumbrical muscles dissected, and NMJs immunolabelled as previously described (Sleigh *et al.*, 2014). Muscles were dissected in cold phosphate-buffered saline (PBS) and fixed in freshly prepared 4% paraformaldehyde (PFA; Electron Microscopy Sciences) in PBS for 10 min. Whole muscles were permeabilised with 2% Triton X-100 in PBS for 30 min, blocked in 4% bovine serum albumin (BSA) and 1% Triton X-100 in PBS for 30 min and then incubated overnight at 4°C in blocking solution with primary antibodies against neurofilament (2H3; Developmental Studies Hybridoma Bank, 1:50) and synaptic vesicles (SV2; Developmental Studies Hybridoma Bank, 1:100). Muscles were washed 3 × 30 min with PBS prior to incubation for 2 h with AlexaFluor 488 secondary antibody (goat anti-mouse, 1:250, Invitrogen) and 1.5 μg/ml tetramethylrhodamine-labelled α-bungarotoxin (α-BTX; Cambridge Bioscience) in PBS. Muscles were washed 3 × 30 min in PBS and mounted on microscope slides in Vectashield (Vector labs) mounting medium containing DAPI.

NMJs were imaged using a Zeiss LSM 710 microscope. For all images, axons are labelled green (2H3 and SV2) and the post-synaptic endplate labelled red (α-BTX). Only NMJs with clearly visible pre-synaptic axons and terminals were scored. ≥50 NMJs were scored per mouse for polyinnervation, and ≥20 for NMJ area measurements. At each time-point, ≥3 mice per genotype were scored. To measure the NMJ area, the perimeter circumscribing the post-synaptic staining from a maximum intensity Z-stack image (0.65-μm intervals) was drawn by hand and the enclosed surface area measured using ImageJ as described (Bogdanik *et al.*, 2013; Sleigh *et al.*, 2014).

RNA sequencing and transcriptomic analysis

Mice were sacrificed at 3 months of age, following laboratory procedures. Spinal cords were dissected and lumbar regions were isolated and frozen at -80□C in RNALater. RNA was subsequently extracted using Trizol reagent (Life Technologies) and Qiagen miRNeasy kit. RNA integrity was validated using a Bioanalyser (Agilent), with RIN values for all extractions above 8. Samples were prepared with Illumina TruSeq RNA Stranded Sample Prep Kit v2. All sequencing was performed on the Illumina HiSeq HiSeq2000 platform to a read depth of at least 26 million. Paired-end sequencing was performed over 100 cycles.

For data analysis, pipelines available from www.cgat.org were used. In brief, data was checked for contamination and read quality using FastQC (v0.11.2) and FastQ Screen (v0.4.4). Poor quality reads were trimmed using Trimmomatic (v0.32). Reads were mapped against a custom genome containing the BAC sequence, which was based on Ensembl release 78 for Mus musculus. Mapping was done using STAR (v2.4.2a) and mapping quality was

ascertained using Picard tools (v2.6.0) and other metrics. Gene level read counts from coding exons were tallied using FeatureCounts from the Subread package (v1.4.6). Pseudocounts were also obtained using Salmon (v.0.8.2) and processed using tximport (v1.2.0). Expression analysis was carried out using DESeq2 (v1.14.1; R v3.3.0). Splicing analysis was performed on untrimmed reads using rMATS-turbo (v0.1) set to detect splicing differences of at least 1% and DEXSeq (v1.24.0). Permutation analysis was carried out with replacement.

Primary cell culture

Primary motor neurons were isolated from the lumbar spinal cords of E13.5 NTg and TDP43^{WT} and TDP-43^{M337V} hemizygous embryos by p75-neurotrophic receptor immunopanning or by density gradient extraction (Wiese *et al.*, 2010; Beaudet *et al.*, 2015). Briefly, the lumbar region of the spinal cord was dissected from each embryo and enriched on laminincoated plates in neurobasal medium (Invitrogen) supplemented with 10% heat-inactivated horse serum (Sigma) and 5 ng/ml brain derived neurotrophic factor (BDNF; PeproTech) and ciliary neurotrophic factor (CNTF; PeproTech). Cultured motor neurons were generally used at 7 days *in vitro* (DIV), except in experiments examining TDP-43 mislocalisation, cell survival or morphology at the timepoints specified. To examine the effect of oxidative stress, motor neurons were treated with 0.05mM sodium arsenite (NaAr; Sigma) in growth media for 0, 30 or 60 minutes. All motor neurons were fixed in 4% paraformaldehyde in PBS, pH 7.2 immediately after treatment. To analyse recovery or survival after NaAr treatment, cells were washed with fresh culture media and allowed to recover for the times specified before fixation. Survival analysis was performed 3 hours after recovery, as either the proportion of surviving cells compared to untreated, or using the MTS assay (Promega)

Mouse embryonic stem cell (ESC)-derived motor neuron culture

Mouse ESC-derived motor neurons were generated from the same ESC lines (IDG26.10-3) originally used to make the TDP-43 BAC mouse. The differentiation protocol was based on previously published work (Bryson *et al.*, 2014; Machado *et al.*, 2014). Briefly, ESCs were expanded on a feeder layer of mouse primary embryonic fibroblasts (PMEFs) in Knockout DMEM (Invitrogen) containing 15% ESC-screened foetal bovine serum (ThermoFisher), 2 mM L-glutamine (Invitrogen), 0.01% MEM non-essential amino acids (Invitrogen), 1 ng/ml leukaemia inhibitory factor (LIF), 0.01% EmbryoMax ESC qualified nucleosides (Millipore) and 0.1 mM 2-mercaptoethanol (Invitrogen). After 2 days, embryoid bodies (EBs) were removed from the underlying PMEF layer by treatment with 0.25% trypsin-EDTA, and the resultant single cell ESC suspension was plated into 10 cm dishes (Nunclon) in ADFNK media (50% advanced DMEM/F-12 (Invitrogen), 50% neurobasal medium (Invitrogen), 10% Knockout serum replacement (Invitrogen), 2 mM L-glutamine (Invitrogen) and 0.1 mM 2mercaptoethanol (Invitrogen). After a further 2 days, EBs were split up to 1:4 into fresh 10 cm dishes in ADFNK containing 1 µM retinoic acid (RA; Sigma) and 0.5 µM smoothened agonist (SAG; Merck). After 3 more days of growth, EBs were collected and dissociated in Accumax (Sigma) and cells plated on laminin-coated plates in ADFNK media containing RA, SAG and growth factors (10ng/ml glia derived neurotrophic factor (GDNF), 10 ng/ml BDNF, 25 ng/ml CNTF and 10 ng/ml NT-3; all from PeproTech). Mature motor neurons were ready for analysis after 2 days.

Immunocytochemistry

Cultured motor neurons were blocked for 1hr at room temperature (RT) with a solution of 5% normal goat serum (NGS) or normal donkey system (NDS) and 0.01% Triton-X 100 in phosphate buffered saline (PBS), and then incubated overnight with primary antibodies. Controls for the specificity of the secondary antibodies had the equivalent amount of antibody solution added, but without any primary antibody. The cells were then washed with PBS, and

incubated for 1hr at RT with secondary antibodies (which were added sequentially to prevent any cross-reaction, particularly between Alexa Fluor-488 donkey anti-goat IgG and Alexa Fluor-568 goat anti-mouse IgG). Cells were mounted using Vectashield hard set mounting medium with DAPI. The primary antibodies used were: rabbit anti-*pan*TDP-43 (to detect both endogenous mouse and exogenous human TDP-43; ProteinTech, Cat. number 10782-2-AP, 1:1000); mouse anti-green fluorescent protein (GFP; Sigma, Cat. number A-11120); goat anti-T-cell internal antigen-1 (TIA-1; Santa Cruz, Cat. number sc-1751, 1:1000), rabbit anti- poly-A binding protein 1 (PABP; Abcam, Cat. number ab21060; 1:1000) and mouse anti-G3BP (Abcam, Cat. number ab56574, 1:1000) (to identify stress granules). Motor neurons were identified by a variety of neuron- and motor neuron-specific markers, including: rabbit anti-βIII-tubulin (Abcam, Cat. number ab15568, 1:1000), mouse ant-SMI32 (BioLegend, Cat. number 801701, 1:1000), mouse anti-Islet1 (Developmental Studies Hybridoma Bank , Cat. number 40.2D6-A, 1:500), mouse anti-Hb9 (Developmental Studies Hybridoma Bank, Cat. number 81.5C10, 1:1000) and goat anti-Choline acetyltransferase (ChAT; Millipore, Cat. number ab144P, 1:500).

Analysis of cells and fluorescence intensity

≥20 random cells were analysed from stained coverslips. At each time-point, ≥3 replicate extractions from embryonic mouse or ESC-derived motor neurons per genotype were scored. Fluorescence intensity measurements were derived from maximum intensity projections generated from z-stacks (0.65μm), to provide maximal nuclear and cytoplasmic area for quantitation of fluorescence distribution and staining intensity. Average relative fluorescence was measured using image J software. Stress granules were identified by immunoreactivity of specific markers (TIA-1, G3BP and PABP) and quantified as a stress granule if ≥ 0.2 μm in size. Stress granule size data was generated by area measurement in Zen lite 2012 software (Zeiss).

Statistical analysis

Repeated measures 2way ANOVA followed by the Bonferroni *post hoc* test was used to compare between wild-type and mutant mouse littermates over time. Kaplan-Meier (LogRank(Mantel-Cox)) survival analysis was used to analyse survival data. NMJs and neuropathological analysis were analysed by one way ANOVA followed by Bonferroni's multiple comparisons test. Transcriptomic analysis is detailed above. Cultured motor neurons were analysed by one way ANOVA followed by Bonferroni's multiple comparisons test, or unpaired t-test where detailed in the text. Two-tailed tests were used in all instances and significance level was $P < 0.05$. Pearson's Correlation was used for co-localisation of TDP43^{M337V} and TIA-1in primary motor neurons, using the colocalisation component of Zen 2012

SP1 software (Zeiss), which is designed for analysis of colocalisation (Manders *et al.*, 1993; Costes *et al.*, 2004). All statistical analysis was carried out using Prism 5 (GraphPad Software, Inc.).

Results

TDP-43^{M337V} mice express low levels of human TDP-43 and develop progressive agedependent motor deficits

We constructed a BAC vector containing the entire genomic sequence of human *TARDBP*, preserving the intron-exon structure and regulatory elements, in order to develop a mouse model of ALS based on relevant and regulated levels of expression of human TDP-43^{M337V}. In ALS patients, the M337V substitution shows clear segregation with the ALS phenotype, is found in geographically unrelated families, and has been used in previous mouse models (Rutherford *et al.*, 2008; Sreedharan *et al.*, 2008). The human genomic insert containing the

mutant allele was integrated into the *Rosa26 (Gt(ROSA26)Sor)* locus in ESCs by PhiC31 integrase mediated cassette exchange to produce a mouse line which, uniquely amongst TDP43 transgenics, expresses a single stable copy of TDP-43^{M337V} with a C-terminal fluorescent tag (Ypet) (Fig. 1A). A mouse line expressing wild-type human TDP-43, constructed in an identical way, served as an important independent control throughout this study.
Immunoblotting of total protein lysates from candidate ESCs with a *pan*TDP-43 antibody that detects mouse and human TDP-43 with equal affinity identified human TDP-43 protein expression (detectable at 72kDa due to the Ypet tag) at a level below that of endogenous mouse Tdp-43 (Fig. 1B). Attempts to generate either TDP-43^{WT} or TDP-43^{M337V} mice on a null *Tardbp* background, by crossing with a *Tardbp*$^{+/-}$ mouse (B6;129P2-*Tardbp*$^{Gt(RRB030)Byg}$/J, The Jackson Laboratory, Cat. Number JAX#012850,), produced no live offspring. This is consistent with previous reports that homozygous null *Tardbp* -/- embryos die between 3.5 and 8.5 days of development (Sephton *et al.*, 2010).

Immunohistochemical staining of 3-month old mouse spinal cord with antibodies against human TDP-43 or GFP (which efficiently detects YPet) confirmed a normal pattern of cellular distribution in both TDP-43$^{WT/-}$ or TDP-43$^{M337V/-}$ animals, in which TDP-43 is predominantly nuclear (Fig. 1C, top *panel*). TDP-43 was expressed at similarly low levels across all tissues examined (Fig. 1C, *bottom panel*). Immunoblotting of cerebral cortex and lumbar spinal cord lysates with a *pan*TDP-43 antibody, confirmed that human TDP-43 is expressed at levels considerably lower than endogenous Tdp-43, and showed no significant difference between hemizygous or homozygous TDP-43 BAC mice (Fig. 1D).

TDP-43$^{M337V/M337V}$ mice displayed a slight, but significant, reduction in weight compared to non-transgenic and TDP-43^{WT} controls, but while this occurred from early in development in male animals (Fig. 2A, *P<0.05, **P<0.01, ***P<0.001, ****P<0.0001) it only occurred by 18 months of age in female animals (Fig. 2B, *P<0.05). These minor weight differences were non-progressive, suggesting weight loss is not an intrinsic feature of the disease phenotype. Combining data from heterozygous and homozygous mice we observed an approximately 50% reduction in survival in TDP-43$^{M337V/M337V}$ mice by 2 years, compared to TDP-43^{WT} and NTg mice (Fig. 2C, Supp. Fig. 1A, B). This difference remained statistically significant when hemizygous and homozygous mutants were analysed independently (*P<0.05 and **P<0.005, respectively), with TDP-43$^{M337V/M337V}$ mice displaying a combined (male and female) median survival of 694 days. Mutant mice also demonstrated progressive, 'dosedependent' loss of motor function. Combined male and female data showed that TDP-43^{M337V} mice display a progressive loss in the ability to stay on an accelerating rotarod, beginning between 6 and 9 months of age (Fig. 2D, Supp. Fig. 1C, D) and progressing through to 18 months (**P<0.01, ***P<0.001, ****P<0.0001). Analysis of combined sex data (Fig. 2E; *P<0.05 and ****P<0.0001, Supp. Fig. 1E, F) confirmed that mutants displayed dosedependent progressive reductions in grip strength beginning between 6-9 months, compared to NTg controls. Mouse weight had no effect on the progressive reduction of grip strength observed in mutant mice (Supp. Fig. 2). Total activity of TDP-43$^{M337V/-}$ and TDP43$^{M337V/M337V}$ mice (male and female combined) was reduced at 12 months in open field testing, indicating that general motor activity and novel exploration was reduced in mutant mice (Fig. 2F; **P<0.01,***P<0.001, ****P<0.001, Supp. Fig. 1G, H). Importantly, mice expressing wild-type human TDP-43 are indistinguishable from non-transgenic littermate controls on all tests of motor function, demonstrating that the motor defects observed are due to expression of the M337V mutant TDP-43 transgene, and are independent of the YPet tag.

Progressive weakness and loss of neuromuscular junction integrity occurs in the absence of cytoplasmic aggregates in TDP-43^{M337V} mice

Other ALS mouse models, notably SOD1^{G93A}, show abnormal NMJ morphology prior to motor neuron axonal and cell body degeneration (Fischer *et al.*, 2004; Cappello *et al.*, 2012). To view neuromuscular junctions in our TDP-43 model, pre-synaptic axons and motor neuron terminals were labelled with antibodies against neurofilament (2H3) and synaptic vesicle (SV2) proteins, and the post-synaptic acetylcholine receptors identified with TRITCconjugated α-bungarotoxin (α-BTX). In 9-month old TDP-43^{M337V} mice, both hemizygous and homozygous, lumbrical neuromuscular endplates (Fig. 3A) displayed reduced size and complexity compared to non-transgenic and TDP-43^{WT} controls. In pre-symptomatic mice (3 months), no significant difference in post-synaptic area was observed (Fig. 3B). At 9 and 12 months of age, there was a significant decrease in post-synaptic area observed in TDP-43$^{M337V/M337V}$ mouse lumbrical muscle compared to control NMJs (Fig. 3B, **P*<0.05). Conversely, no significant differences were observed in gastrocnemius muscle at symptomatic timepoints (Fig. 3C). In tandem with the development of motor dysfunction in these mice we observed increased partial denervation. Representative lumbrical NMJs are shown from 12 month NTg, TDP-43^{WT} and TDP-43^{M337V} mice (Fig. 3D). At 12 months of age we identified a significant increase in the number of partially denervated NMJs in TDP43$^{M337V/M337V}$ homozygous mouse lumbrical muscles compared to controls (Fig. 3E, **P*<0.05), which was confirmed by the significant loss of synaptic overlap between the area of axonal immunostaining (2H3/SV2) and that of the endplate (α-BTX) at this timepoint (Fig. 3F, **P*<0.05). As with post-synaptic area, there were no significant changes to synaptic overlap observed in the gastrocnemius at 12 months (Fig. 3G).

Mislocalisation of TDP-43 from the nucleus and incorporation into cytoplasmic aggregates is observed at autopsy in CNS tissue in ALS and FTD patients. Whether this is a core part of the mechanism of neurodegeneration in ALS, is secondary to upstream initiators of disease, or is a neutral or even protective phenomenon, is unclear (Neumann *et al.*, 2006; Buratti and Baralle, 2012). At no timepoint, up to 24 months of age, in hemizygous and homozygous TDP-43^{M337V} lumbar spinal cord, did we observe evidence of nuclear clearing or cytoplasmic accumulation of TDP-43, using GFP or *pan*TDP-43 immunoreactivity (Fig. 4A, Supp. Fig. 3A,B). There was also no evidence for significant neuronal death or macrophage/microglial involvement, as evidenced by NeuN (Fig. 4A, B) or Iba1 immunoreactivity (Fig. 4A, C), respectively. Similarly, there was no significant evidence of p62 or phosphorylated TDP-43 accumulation, in the spinal cord of mutant mice at 12 months (Fig. 4D). Similarly, we could not find evidence of altered neurofilament or peripherin expression in our either mutant or wildtype human TDP-43 BAC transgenic mice at 24 months (Supp. Fig 3C).

ALS-associated mutant forms of TDP-43 have a propensity to aggregate and become enriched in insoluble fractions (Johnson *et al.*, 2009). In this model we find that mutant human TDP-43 protein levels are elevated in pre-symptomatic and symptomatic TDP43^{M337V} mouse CNS, in the absence of TDP-43 cytoplasmic aggregates. Immunoblot analysis of soluble and insoluble (urea-soluble) protein lysates from pre-symptomatic (3 months) mouse CNS indicates elevation of insoluble mutant human TDP-43 in the brain of homozygous mice only compared to wild-type TDP-43 controls (Supp. Fig. 4B, C, $^{**}P<0.05$). In symptomatic mice (9 months) human mutant TDP-43 was elevated in both soluble and insoluble protein

fractions of TDP-43^{M337V} homozygous cortex (Supp. Fig. 5B, *P and **P<0.05) and spinal cord (Supp. Fig. 5C, **P<0.05). Human TDP-43 was elevated in both fractions from TDP-43^{WT} cortex (*P and **P<0.05), but did not reach significance in spinal cord lysates. Increased protein expression of human mutant TDP-43 in insoluble fractions is consistent with the idea that TDP-43 accumulates in detergent resistant fractions, and might ultimately form aggregates (Johnson *et al.*, 2009; Li *et al.*, 2013). Human TDP-43 transcript levels are significantly increased in homozygous mouse brain and spinal cord at 3 months of age, compared to hemizygous mice (Supp. Fig. 6A, B, (*P<0.05 and **P<0.05), without any phenotype, but by 9 months, are equivalent across TDP-43^{WT} and TDP-43^{M337V} mouse CNS. This suggests that progressive accumulation of protein may downregulate the human transcript, consistent with the known effect of TDP-43 in auto-regulating its own levels (Polymenidou *et al.*, 2011).

Substantial splicing events are not detected in the pre-symptomatic phase of ALS pathogenesis in TDP-43^{M337V} mice.

TDP-43 is known to modulate the splicing of thousands of widely expressed transcripts (Polymenidou *et al.*, 2011). If loss of the splicing function of TDP-43 is a primary driver of the disease mechanism in ALS, and it is present at a level which can be detected, it should therefore logically be present before clinical and pathological disease onset. We therefore sought to test whether differences in splicing contribute to the development of pathophysiology in the M337V mouse model. RNA sequencing was performed on RNA extracted from whole lumbar spinal cord of 3-month old female mice (hemizygous TDP43^{M337V}, n=5, hemizygous TDP-43^{WT} mice, n=3, NTg mice, n=2). Quality control did not reveal systematic biases: read depth was 28.6 million reads (SD 0.7 million), median 5' to

3' bias from picard was 0.74 (SD 0.04) and GC content was 46.4 % (SD 0.5%) and was not significantly different between samples. Exploratory data analysis of gene expression using principal component analysis revealed that principal component 1 separated M337 from both NTg and transgenic mice and accounted for 33% of the total variance (Fig. 5A). Differential exon events were assessed in M337V versus non-mutant animals. rMATS analysed 57,411 exon usage events, of which only 48 were different between the conditions (FDR threshold 0.05). Permutation of group labels revealed that these events were likely to be nonspecific (Fig. 5B; p = 34/100). The lack of splicing differences in the mutant M337V mouse at three months was further corroborated using DEXSeq, which found only two statistically significant differential exon usage events in this cohort. Therefore, we could not detect sizable differences in splicing events in this analysis, within the constraints of read depth and sample size.

Differential expression reveals a modest but distinct transcription profile in presymptomatic TDP-43M337V/- mouse spinal cord

Differential expression analysis was carried out on the same five female TDP-43$^{M337V/-}$ mice versus five female controls (a combination of NTg and TDP-43$^{WT/-}$ mice). On gene-level differential expression analysis using DESeq2, 633 genes were differentially expressed between 3-month old M337V mutant mice and non-mutant animals, using a BenjaminiHochburg adjusted p value cut-off of 0.05 and a log-fold change threshold of 0.2. Most of these changes were below the magnitude accepted for RNA sequencing experiments of this scale: No log2-fold expression changes above 0.6 or below -0.8 were observed (Figure 5C). Despite the modest changes, permutation analysis of genotype labels validated the specificity of the findings (Fig. 5D, *P*=0.007). To functionally characterise the results a

Phenotypic Linkage Network Analysis was performed on a nervous system specific network (Honti *et al.*, 2014). There was a more than two-fold enrichment of functional connections in the differentially expressed genes compared to genes randomly drawn from the network (Fig. 5E, $P<0.001$). Subnetwork analysis discovered discrete modules that were found to be related to cellular functions relevant to motor neuron biology (Table 2). Interestingly, the only ALS/FTD related gene that was differentially expressed was progranulin, which was downregulated in the TDP-43^{M337V} mouse.

TDP-43$^{M337V/-}$ cytoplasmic redistribution in primary motor neurons is associated with altered stress granule dynamics

In order to investigate the cellular behaviour of mutant human TDP-43 we cultured spinal motor neurons from E13.5 mice, which were identified with the motor neuron marker SMI32 (Supp. Fig. 7A). In resting (unstressed) conditions, the distribution of TDP-43 in the motor neurons hemizygously expressing wild-type human TDP-43 was identical to that seen in non-transgenic mice, following immunostaining with the *pan*TDP-43 antibody (Fig. 6A). TDP-43 was predominantly located in the nucleus in the majority of motor neurons analysed, with more low-level diffuse cytoplasmic staining. In contrast, the majority of primary motor neurons derived from hemizygously expressing TDP-43$^{M337V/-}$ spinal cord displayed spontaneous cytoplasmic mis-localisation of the total pool of exogenous and endogenous TDP-43 under basal conditions (Fig. 6A, 6B, $*P<0.05$). To examine temporal progression of TDP-43 cytoplasmic mis-localisation, motor neurons from NTg and TDP-43$^{M337V/-}$ lines were fixed and stained with *pan*TDP-43 (Fig. 6C). Beginning at 3DIV, there is a significant increase in the number of TDP-43$^{M337V/-}$ motor neurons displaying cytoplasmic TDP-43 mislocalisation ($**P<0.01$). To confirm the re-distribution of TDP-43 in TDP-43$^{M337V/-}$ motor neurons, we

compared total cellular TDP-43 fluorescence intensity between the nucleus and cytoplasm in maximum intensity projections generated from z-stacks. We identified that there was significantly more *pan*TDP-43 in the cytoplasm of TDP-43$^{M337V/-}$ primary motor neurons under basal conditions, compared to non-transgenic and TDP-43$^{WT/-}$ controls (Fig. 6D, **P*<0.05).

Accumulation of *pan*TDP-43 fluorescence in the cytoplasmic compartment occurs as early as 3DIV (Fig. 6E, ***P*<0.01). Immunoblotting with *pan*TDP-43 after nuclear/cytoplasmic fractionation confirmed the accumulation of human TDP-43 in the TDP-43$^{M337V/-}$ cytoplasmic compartment (Fig. 6F). We next analysed spinal cord motor neurons using a GFP antibody directed against the C-terminal Ypet tag, to observe the human-specific pool of TDP-43 within the cells (Fig. 6G). Ypet is a ~30kDa green fluorescent protein (GFP)-derivative that demonstrates excellent photostability, increased brightness compared to GFP and falls within the commonly used Fluorescein isothiocyanate (FITC) excitation/emission filter set (Nguyen and Daugherty, 2005; Alegre-Abarrategui *et al.*, 2009). The number of mutant motor neurons displaying cytoplasmic mislocalisation of human TDP-43 (Fig. 6H, **P*<0.05), and the accumulation of human TDP-43 fluorescence in the mutant cell cytoplasm (Fig. 6I, **P*<0.05), were significantly increased compared to TDP-43^{WT} controls. The Z Factor[1] for the cytoplasmic localization of *pan*TDP-43 between TDP-43$^{WT/-}$ and TDP-43$^{M337V/-}$ motor neurons is 0.65, which suggests the readout is robust.

Stress granules are cytoplasmic foci in which mRNAs for housekeeping proteins are stored and translationally repressed, allowing the selective translation of stress-response proteins (e.g.heat shock proteins) (Bentmann *et al.*, 2013; Li *et al.*, 2013). TDP-43 is recruited to stress granules and some reports have suggested that mutant TDP-43 may disturb stress granule formation (McDonald *et al.*, 2011; Colombrita *et al.*, 2012). However, these studies have been confounded by the potential effects of overexpression and transfection. We

therefore took advantage of the lower levels of human TDP-43 expression in our model to investigate the effect of mutant TDP-43 expression on stress granule formation in primary embryonic motor neurons. Stress granules were identified with antibodies directed against TIA-1 (Fig. 7A), G3BP and PABP (Bentmann *et al.*, 2013), and included if ≥ 0.2 μm in size. In response to increasing time of exposure to sodium arsenite, to induce oxidative stress, the proportion of TDP-43^{WT} hemizygous motor neurons forming stress granules was indistinguishable from that seen in NTg controls, whether identified by TIA-1, G3BP or PABP (Fig. 7B) immunoreactivity. However, in mutant TDP-43-derived motor neurons we observed a significant reduction in the number of cells containing stress granules compared to NTg controls after 60 minutes of exposure (TIA-1, G3BP and PABP) (7B, **P*<0.05). G3BPpositive stress granules are also significantly smaller in TDP-43$^{M337V/-}$ motor neurons compared to TDP-43$^{WT/-}$ motor neurons, when we quantified the area of individual SGs (Fig. 7C, 7D, ****P*<0.0001). Similar stress granule size reductions were observed after quantifying the size of individual PABP-positive granules in TDP-43$^{M337V/-}$ motor neurons (7E, 7F **P*<0.05).

The molecular mechanisms by which mutations in TDP-43 might lead to a reduction in stress granule formation are still unclear (Li *et al.*, 2013), though knockdown of TDP-43 leads to impaired stress granule assembly in cell lines, suggesting TDP-43 is an important component of stress granule function (Aulas and Vande Velde, 2015). To further examine the relationship between mutant human TDP-43 and stress granules, we examined co-localisation using Pearson's coefficient to measure of the linear correlation between fluorescent staining (Manders *et al.*, 1993; Costes *et al.*, 2004). Motor neurons generated from TDP-43^{WT} and TDP-43^{M337V} mice were exposed to NaAr to induce oxidative stress, then immunostained with antibodies against GFP, to identify the human TDP-43 pool, and TIA-1. Co-localisation

between GFP and TIA-1 is significantly reduced in the cytoplasm of stress-granule positive TDP-43^{M337V} motor neurons compared to TDP-43^{WT} controls following 0, 30 or 60 min exposure to sodium arsenite (Fig. 7G, *P<0.05). We only chose stress granule-positive motor neurons for this analysis to confirm that the apparent reduced association between GFP and TIA-1 was not simply due to the observed reduction in the number of mutant motor neurons containing stress granules. When we analysed recovery from NaAr treatment only in stress granule-positive motor neurons, we found that stress granule disassembly appeared normal, suggesting that stress granule impairment in these mutant cells is associated with assembly rather than dis-aggregation (Fig. 7H, *P<0.05). In response to increasing NaAr exposure, followed by 3 hours recovery from oxidative stress, TDP-43$^{M337V/-}$ motor neurons displayed reduced survival compared to controls at 7DIV (Fig. 7I, *P<0.05).

To determine if the phenotypic changes we were observing in primary motor neurons are a general phenomenon in motor neurons, we explored stress granule dynamics using motor neurons generated from the ESC lines originally used to generate our TDP-43 mice. These ESC-derived motor neurons express a battery of common motor neuron markers (Supp. Fig. 7B, C). NTg and TDP-43$^{WT/-}$ mouse ESC-derived motor neurons displayed no difference in their ability to produce stress granules with increasing exposure to NaAr. However, after 60 min of exposure to NaAr, the number of stress granules is reduced in mutant-containing cells (Fig. 7J, representative G3BP immunostaining). The presence of TDP-43^{M337V} leads to a significant reduction in the proportion of motor neurons containing G3BP and PABP-positive stress granules after 60 min exposure to NaAr (Fig. 7K, *P<0.05). When we quantified the number of stress granules per cell, we found a significant reduction in the number of G3BP- and PABP-positive stress granules within TDP-43^{M337V} ESC-motor neurons (Fig. 7L, **P<0.01, ***P<0.001). TDP-43$^{M337V/-}$ ESC-derived motor neurons display reduced survival

following NaAr exposure at 2DIV compared to controls (Fig. 7M)*P<0.05). These data suggest that mutant TDP-43 cytoplasmic mislocalisation may alter cell viability thorough altering the stress granule response in conditions such as oxidative stress, providing at least one possible pathological mechanism whereby mutant TDP-43 might render motor neurons vulnerable in ALS. Analysis of cortical neurons from the TDP-43$^{M337V/-}$ mouse indicated they do not recapitulate the TDP-43 phenotype observed in motor neuron populations (Supp. Fig. 8).

Discussion

Models based on transgenic overexpression of Cu/Zn superoxide dismutase-1 (SOD1), the first gene to be associated with familial ALS (Rosen, 1993), have shed light on many of the biochemical and molecular pathways that underlie motor neuron degeneration, but have not yet led to disease modifying treatments (Rosen *et al.*, 1993; Bensimon *et al.*, 1994; Andersen, 2006; Swarup and Julien, 2011). This may be due to fundamental differences in the biology of SOD1-associated ALS, which is notable for the absence of TDP-43 pathology, or reflect a problem with using transgenic models in which mutant protein is expressed at supraphysiological levels. Previous models based on TDP-43 overexpression or expression driven by non-physiological promoters have produced variable results that could reflect nonspecific pathways, given that mutant and wild were often equally toxic in these models (Wegorzewska *et al.*, 2009; Shan *et al.*, 2010; Stallings *et al.*, 2010; Tsai *et al.*, 2010; Wils *et al.*, 2010; Xu *et al.*, 2010; Xu *et al.*, 2011).

In this study we report the generation of a novel mouse model of ALS/FTD based on the low-level expression of an ALS-associated human TDP-43 mutation (M337V) driven by the

endogenous human promoter, from a construct with intact introns and downstream regulatory elements. We show that this low level expression of an ALS-associated mutant leads to progressive weakness in the absence of TDP-43 insoluble aggregates or neuroinflammation, and that this phenotype is not primarily driven by generalised alteration in splicing. *In vitro* observations indicate that mutant TDP-43 is associated with a reproducible deficit in stress granule assembly.

TDP-43 gene deletion leads to early embryonic lethality (Wu *et al.*, 2010). We were unable to generate either TDP-43^{WT} or TDP-43^{M337V} mice on a null *Tardbp* background. This may be due to a failure of human TDP-43 to functionally replace the mouse gene, or because the levels of transgene expression were too low (Wu *et al.*, 2010). However, expressing the human mutation on a background of normal mouse Tdp-43 levels allows us to explore the specific toxicity of the human mutation without the potentially confounding effects of lossof-function. Heterozygous and homozygous TDP-43^{M337V} BAC mice develop late-onset, agedependent and progressive motor function deficits identified by reduced grip strength and a reduced latency to fall from the accelerating rotarod, with homozygous mice performing significantly worse than heterozygous littermates. This dose-dependent affect is also reflected in reduced survival of homozygous mutants compared to hemizygotes. We also observed elevated levels of mutant human TDP-43 in the cortex and spinal cord of pre-symptomatic TDP-43^{M337V} homozygous mice compared to TDP-43^{WT} controls, particularly in the insoluble protein fraction. The absence of cytoplasmic aggregation of TDP-43 in symptomatic lumbar spinal cord motor neurons, suggest that, as in other mouse models, aggregation is not necessary for disease initiation (Janssens *et al.*, 2013). In contrast to SOD1-based mouse models of ALS, in which neuroinflammation is a prominent feature, we did not observe activation of microglia. This is in agreement with recent studies, in which microglia have

even been implicated as a protective factor, inhibited by the presence of human TDP-43 mutations (Spiller *et al.*, 2018).

The decrease in NMJ area and increase in partial denervation of the synapse in TDP-43^{M337V} homozygotes is consistent with the motor function deficits observed, especially considering that lumbrical muscles are directly involved in grip strength and locomotion. Previous studies from Drosophila have reported that mutant TDP-43 can influence NMJ morphology, pre- and post-synaptically via the modulation of synaptic microtubule organization via microtubule associated proteins (Feiguin *et al.*, 2009; Godena *et al.*, 2011; Chang and Morton, 2017). In mouse studies, evidence suggests abnormalities in NMJ structure might lead to functional changes, which ultimately affect the fidelity of synaptic transmission, therefore contributing to the ALS phenotype (Rocha *et al.*, 2013). Further work is required to understand the temporal relationship between the motor phenotype and denervation, especially analysis of potential axonal transport deficits, progressive neuromuscular weakness occurs in the absence of altered splicing or cytoplasmic aggregation, indicating that potentially reversible abnormalities might precede cell death. Importantly, we have developed a mouse model in which the neuromuscular system develops normally and is well established, before the onset of neurodegeneration, which occurs over a timescale akin to that seen in human ALS.

Although it is generally assumed that toxicity from TDP-43 due either to specific genetic mutations in familial ALS or mislocalisation in sporadic ALS is key to pathophysiology, there is ongoing debate about the role of loss of function of TDP-43. Here, we have shown that prior to disease onset there is no evidence of a generalised alteration in the constitutive splicing function of TDP-43, though this may contribute to late pathology. In contrast, altered

expression of specific pathways is revealed by RNA expression studies, will facilitate further work, in particular whether these changes drive loss of synaptic integrity, an early feature of our model.

We have established that primary and ESC-derived motor neurons have a complement of ALS-relevant phenotypes. In resting (unstressed) conditions, a significantly higher proportion of primary motor neurons from TDP-43^{M337V} mice display consistent and significant cytoplasmic mis-localisation of TDP-43 from its normal nuclear distribution (Fig. 6), with temporal analysis indicating that the phenotype can appear as early as 3DIV after plating neural precursors. Experiments in primary neurons indicate that an acquired alteration in stress granule function is specific to mutant TDP-43 (Fig. 7), with no phenotypic deficits observed in TDP-43^{WT} cells or tissues. While this suggests that in this model the mutation serves to promote cytoplasmic mislocalisation of TDP-43, we note that this was not clearly detectable *in vivo* in spinal cord motor neurons in otherwise symptomatic adult mutant mice. Possible explanations for this include the modifying effect of non-neuronal cells in the whole spinal cord, or that the presence of immunodetectable aggregates occurs downstream of the events which initiate the pathophysiology of ALS. It is possible that the alterations in TDP-43 distribution seen in cell culture occur *in vivo* but are below the detection threshold of immunohistochemical methods.

In summary, we have generated a new mouse model of ALS which demonstrates that overexpression of mutant TDP-43 is not required to produce a clear phenotype and reduction in survival. Critically, this model displays two key phenotypic features that will facilitate future study. First, progressive motor dysfunction occurs over a timescale akin to that seen in

human ALS and develops after the establishment of a mature neuromuscular system. This has the potential to allow the identification of key early changes in cellular pathology occurring in the pre-symptomatic phase of ALS and therefore might generate more therapeutically tractable targets. Secondly, primary motor neurons from the mouse provide a valuable *in vitro* tool for further exploration of the role of TDP-43 cytoplasmic mislocalisation, alteration in stress granule dynamics in ALS and for compound screening. This mouse model adds to the accumulating evidence, including the recent identification of mutations in TIA-1 as a rare cause of the disease, that stress granules might be a key site of ALS pathogenesis (Mackenzie *et al.*). The demonstration of reproducible *in vitro* and *in vivo* phenotypes will facilitate testing of potential therapies using high-throughput screens based on abrogation of disease-altered stress granule dynamics.

Acknowledgements

This work was funded by a research grant from the MND Association. RD was the recipient of an MND Association PhD Studentship, JS held a Lady Edith Wolfson MND Association/Medical Research Council Clinical Training Fellowship, and LK was the recipient of an Association of British Neurologists/Patrick Berthould Clinical Fellowship. BD and DB were supported by the Wellcome Trust [203141/Z/16/Z].

References

Al-Chalabi A, Calvo A, Chio A, Colville S, Ellis CM, Hardiman O, *et al.* Analysis of amyotrophic lateral sclerosis as a multistep process: a population-based modelling study. The Lancet Neurology 2014; 13(11): 1108-13.

Alegre-Abarrategui J, Christian H, Lufino MM, Mutihac R, Venda LL, Ansorge O, *et al.* LRRK2 regulates autophagic activity and localizes to specific membrane microdomains in a novel human genomic reporter cellular model. Hum Mol Genet 2009; 18(21): 4022-34.

Andersen PM. Amyotrophic lateral sclerosis associated with mutations in the CuZn superoxide dismutase gene. Curr Neurol Neurosci Rep 2006; 6(1): 37-46.

Arai T, Hasegawa M, Akiyama H, Ikeda K, Nonaka T, Mori H, *et al.* TDP-43 is a component of ubiquitin-positive tau-negative inclusions in frontotemporal lobar degeneration and amyotrophic lateral sclerosis. Biochem Biophys Res Commun 2006; 351(3): 602-11. Aulas A, Vande Velde C. Alterations in stress granule dynamics driven by TDP-43 and FUS: a link to pathological inclusions in ALS? Frontiers in Cellular Neuroscience 2015; 9(423). Beaudet M-J, Yang Q, Cadau S, Blais M, Bellenfant S, Gros-Louis F, *et al.* High yield extraction of pure spinal motor neurons, astrocytes and microglia from single embryo and adult mouse spinal cord. Scientific Reports 2015; 5: 16763.

Bensimon G, Lacomblez L, Meininger V. A controlled trial of riluzole in amyotrophic lateral sclerosis. ALS/Riluzole Study Group. N Engl J Med 1994; 330(9): 585-91.

Bentmann E, Haass C, Dormann D. Stress Granules in Neurodegeneration - Lessons learnt from TDP-43 and FUS. FEBS Journal 2013: n/a-n/a.

Bogdanik LP, Sleigh JN, Tian C, Samuels ME, Bedard K, Seburn KL, *et al.* Loss of the E3 ubiquitin ligase LRSAM1 sensitizes peripheral axons to degeneration in a mouse model of Charcot-Marie-Tooth disease. Dis Model Mech 2013; 6(3): 780-92.

Bryson JB, Machado CB, Crossley M, Stevenson D, Bros-Facer V, Burrone J, *et al.* Optical

Control of Muscle Function by Transplantation of Stem Cell–Derived Motor Neurons in Mice. Science 2014; 344(6179): 94-7.

Buratti E, Baralle FE. TDP-43: gumming up neurons through protein-protein and proteinRNA interactions. Trends Biochem Sci 2012; 37(6): 237-47.

Cairns NJ, Neumann M, Bigio EH, Holm IE, Troost D, Hatanpaa KJ, *et al.* TDP-43 in familial and sporadic frontotemporal lobar degeneration with ubiquitin inclusions. Am J Pathol 2007; 171(1): 227-40.

Cappello V, Vezzoli E, Righi M, Fossati M, Mariotti R, Crespi A, *et al.* Analysis of neuromuscular junctions and effects of anabolic steroid administration in the SOD1G93A mouse model of ALS. Molecular and Cellular Neuroscience 2012; 51(1–2): 12-21. Chang J-C, Morton DB. Drosophila lines with mutant and wild type human TDP-43 replacing the endogenous gene reveals phosphorylation and ubiquitination in mutant lines in the absence of viability or lifespan defects. PLOS ONE 2017; 12(7): e0180828.

Chen CM, Krohn J, Bhattacharya S, Davies B. A comparison of exogenous promoter activity at the ROSA26 locus using a PhiiC31 integrase mediated cassette exchange approach in mouse ES cells. PLoS One 2011; 6(8): e23376.

Colombrita C, Onesto E, Megiorni F, Pizzuti A, Baralle FE, Buratti E, *et al.* TDP-43 and FUS RNA-binding proteins bind distinct sets of cytoplasmic messenger RNAs and differently regulate their post-transcriptional fate in motoneuron-like cells. J Biol Chem 2012; 287(19): 15635-47.

Costes SV, Daelemans D, Cho EH, Dobbin Z, Pavlakis G, Lockett S. Automatic and Quantitative Measurement of Protein-Protein Colocalization in Live Cells. Biophysical Journal 2004; 86(6): 3993-4003.

Da Cruz S, Cleveland DW. Understanding the role of TDP-43 and FUS/TLS in ALS and beyond. Curr Opin Neurobiol 2011.

Feiguin F, Godena VK, Romano G, D'Ambrogio A, Klima R, Baralle FE. Depletion of TDP43 affects Drosophila motoneurons terminal synapsis and locomotive behavior. FEBS Lett
2009; 583(10): 1586-92.

Fischer LR, Culver DG, Tennant P, Davis AA, Wang M, Castellano-Sanchez A, *et al.* Amyotrophic lateral sclerosis is a distal axonopathy: evidence in mice and man. Experimental Neurology 2004; 185(2): 232-40.

Gitcho MA, Baloh RH, Chakraverty S, Mayo K, Norton JB, Levitch D, *et al.* TDP-43 A315T mutation in familial motor neuron disease. Ann Neurol 2008; 63(4): 535-8. Godena VK, Romano G, Romano M, Appocher C, Klima R, Buratti E, *et al.* TDP-43 regulates Drosophila neuromuscular junctions growth by modulating Futsch/MAP1B levels and synaptic microtubules organization. PLoS One 2011; 6(3): e17808.

Hasegawa M, Arai T, Nonaka T, Kametani F, Yoshida M, Hashizume Y, *et al.* Phosphorylated TDP-43 in frontotemporal lobar degeneration and amyotrophic lateral sclerosis. Ann Neurol 2008; 64(1): 60-70.

Honti F, Meader S, Webber C. Unbiased Functional Clustering of Gene Variants with a Phenotypic-Linkage Network. PLOS Computational Biology 2014; 10(8): e1003815.

Janssens J, Van Broeckhoven C. Pathological mechanisms underlying TDP-43 driven neurodegeneration in FTLD–ALS spectrum disorders. Human Molecular Genetics 2013; 22(R1): R77-R87.

Janssens J, Wils H, Kleinberger G, Joris G, Cuijt I, Ceuterick-de Groote C, *et al.* Overexpression of ALS-Associated p.M337V Human TDP-43 in Mice Worsens Disease Features Compared to Wild-type Human TDP-43 Mice. Mol Neurobiol 2013; 48(1): 22-35.

Johnson BS, Snead D, Lee JJ, McCaffery JM, Shorter J, Gitler AD. TDP-43 Is Intrinsically

Aggregation-prone, and Amyotrophic Lateral Sclerosis-linked Mutations Accelerate Aggregation and Increase Toxicity. Journal of Biological Chemistry 2009; 284(30): 20329-39.

Kabashi E, Valdmanis PN, Dion P, Spiegelman D, McConkey BJ, Vande Velde C, *et al.* TARDBP mutations in individuals with sporadic and familial amyotrophic lateral sclerosis. Nat Genet 2008; 40(5): 572-4.

Lagier-Tourenne C, Polymenidou M, Cleveland DW. TDP-43 and FUS/TLS: emerging roles in RNA processing and neurodegeneration. Hum Mol Genet 2010; 19(R1): R46-64.

Li YR, King OD, Shorter J, Gitler AD. Stress granules as crucibles of ALS pathogenesis. The Journal of Cell Biology 2013; 201(3): 361-72.

Livak KJ, Schmittgen TD. Analysis of Relative Gene Expression Data Using Real-Time Quantitative PCR and the 2−ΔΔCT Method. Methods 2001; 25(4): 402-8.

Machado CB, Kanning KC, Kreis P, Stevenson D, Crossley M, Nowak M, *et al.* Reconstruction of phrenic neuron identity in embryonic stem cell-derived motor neurons. Development 2014; 141(4): 784-94.

Mackenzie IR, Nicholson AM, Sarkar M, Messing J, Purice MD, Pottier C, *et al.* TIA1 Mutations in Amyotrophic Lateral Sclerosis and Frontotemporal Dementia Promote Phase Separation and Alter Stress Granule Dynamics. Neuron 2017; 95(4): 808-16.e9.

Manders EMM, Verbeek FJ, Aten JA. Measurement of co-localization of objects in dualcolour confocal images. Journal of Microscopy 1993; 169(3): 375-82.

McDonald KK, Aulas A, Destroismaisons L, Pickles S, Beleac E, Camu W, *et al.* TAR DNAbinding protein 43 (TDP-43) regulates stress granule dynamics via differential regulation of G3BP and TIA-1. Hum Mol Genet 2011; 20(7): 1400-10.

Mutihac R, Alegre-Abarrategui J, Gordon D, Farrimond L, Yamasaki-Mann M, Talbot K, *et al.* TARDBP pathogenic mutations increase cytoplasmic translocation of TDP-43 and cause

reduction of endoplasmic reticulum Ca2 + signaling in motor neurons. Neurobiology of Disease 2015; 75(0): 64-77.

Neumann M, Sampathu DM, Kwong LK, Truax AC, Micsenyi MC, Chou TT, *et al.* Ubiquitinated TDP-43 in Frontotemporal Lobar Degeneration and Amyotrophic Lateral Sclerosis. Science 2006; 314(5796): 130-3.

Nguyen AW, Daugherty PS. Evolutionary optimization of fluorescent proteins for intracellular FRET. Nature Biotechnology 2005; 23: 355.

Polymenidou M, Lagier-Tourenne C, Hutt KR, Huelga SC, Moran J, Liang TY, *et al.* Long pre-mRNA depletion and RNA missplicing contribute to neuronal vulnerability from loss of TDP-43. Nat Neurosci 2011.

Rocha MC, Pousinha PA, Correia AM, Sebastiao AM, Ribeiro JA. Early changes of neuromuscular transmission in the SOD1(G93A) mice model of ALS start long before motor symptoms onset. PLoS One 2013; 8(9): e73846.

Rosen DR. Mutations in Cu/Zn superoxide dismutase gene are associated with familial amyotrophic lateral sclerosis. Nature 1993; 362: 59-62.

Rosen DR, Siddique T, Patterson D, Figlewicz DA, Sapp P, Hentati A, *et al.* Mutations in Cu/Zn superoxide dismutase gene are associated with familial amyotrophic lateral sclerosis. Nature 1993; 362(6415): 59-62.

Rowland LP, Shneider NA. Amyotrophic Lateral Sclerosis. New England Journal of Medicine 2001; 344(22): 1688-700.

Rutherford NJ, Zhang Y-J, Baker M, Gass JM, Finch NA, Xu Y-F, *et al.* Novel Mutations in TARDBP (TDP-43) in Patients with Familial Amyotrophic Lateral Sclerosis. PLOS Genetics 2008; 4(9): e1000193.

Sephton CF, Good SK, Atkin S, Dewey CM, Mayer P, Herz J, *et al.* TDP-43 Is a Developmentally Regulated Protein Essential for Early Embryonic Development. Journal of Biological Chemistry 2010; 285(9): 6826-34.

Shan X, Chiang PM, Price DL, Wong PC. Altered distributions of Gemini of coiled bodies and mitochondria in motor neurons of TDP-43 transgenic mice. Proc Natl Acad Sci U S A 2010; 107(37): 16325-30.

Sleigh JN, Burgess RW, Gillingwater TH, Cader MZ. Morphological analysis of neuromuscular junction development and degeneration in rodent lumbrical muscles. J Neurosci Methods 2014; 227: 159-65.

Sreedharan J, Blair IP, Tripathi VB, Hu X, Vance C, Rogelj B, *et al.* TDP-43 Mutations in Familial and Sporadic Amyotrophic Lateral Sclerosis. Science 2008; 319(5870): 1668-72.

Stallings NR, Puttaparthi K, Luther CM, Burns DK, Elliott JL. Progressive motor weakness in transgenic mice expressing human TDP-43. Neurobiol Dis 2010; 40(2): 404-14.

Swarup V, Julien JP. ALS pathogenesis: recent insights from genetics and mouse models. Prog Neuropsychopharmacol Biol Psychiatry 2011; 35(2): 363-9.

Talbot K. Motor neuron disease: the bare essentials. Pract Neurol 2009; 9(5): 303-9.

Tsai KJ, Yang CH, Fang YH, Cho KH, Chien WL, Wang WT, *et al.* Elevated expression of TDP-43 in the forebrain of mice is sufficient to cause neurological and pathological phenotypes mimicking FTLD-U. J Exp Med 2010; 207(8): 1661-73.

Van Deerlin VM, Leverenz JB, Bekris LM, Bird TD, Yuan W, Elman LB, *et al.* TARDBP mutations in amyotrophic lateral sclerosis with TDP-43 neuropathology: a genetic and histopathological analysis. The Lancet Neurology 2008; 7(5): 409-16.

Wade-Martins R, Smith ER, Tyminski E, Chiocca EA, Saeki Y. An infectious transfer and expression system for genomic DNA loci in human and mouse cells. Nat Biotechnol 2001; 19(11): 1067-70.

Wang W, Arakawa H, Wang L, Okolo O, Siedlak SL, Jiang Y, *et al.* Motor-Coordinative and Cognitive Dysfunction Caused by Mutant TDP-43 Could Be Reversed by Inhibiting Its Mitochondrial Localization. Molecular Therapy 2017; 25(1): 127-39.

Wegorzewska I, Bell S, Cairns NJ, Miller TM, Baloh RH. TDP-43 mutant transgenic mice develop features of ALS and frontotemporal lobar degeneration. Proc Natl Acad Sci U S A 2009; 106(44): 18809-14.

Wiese S, Herrmann T, Drepper C, Jablonka S, Funk N, Klausmeyer A, *et al.* Isolation and enrichment of embryonic mouse motoneurons from the lumbar spinal cord of individual mouse embryos. Nat Protoc 2010; 5(1): 31-8.

Wils H, Kleinberger G, Janssens J, Pereson S, Joris G, Cuijt I, *et al.* TDP-43 transgenic mice develop spastic paralysis and neuronal inclusions characteristic of ALS and frontotemporal lobar degeneration. Proc Natl Acad Sci U S A 2010; 107(8): 3858-63.

Wu LS, Cheng WC, Hou SC, Yan YT, Jiang ST, Shen CK. TDP-43, a neuro-pathosignature factor, is essential for early mouse embryogenesis. Genesis 2010; 48(1): 56-62.

Xu YF, Gendron TF, Zhang YJ, Lin WL, D'Alton S, Sheng H, *et al.* Wild-type human TDP43 expression causes TDP-43 phosphorylation, mitochondrial aggregation, motor deficits, and early mortality in transgenic mice. J Neurosci 2010; 30(32): 10851-9.

Xu YF, Zhang YJ, Lin WL, Cao X, Stetler C, Dickson DW, *et al.* Expression of mutant TDP-43 induces neuronal dysfunction in transgenic mice. Mol Neurodegener 2011; 6: 73.

Tables

Table 1. Motor function testing cohort.

	Non-transgenic (NTg)	**TDP-43^{WT}/-**	**TDP-43$^{WT/WT}$**	**TDP-43$_{M337V/-}$**	**TDP-43$_{M337V/M337V}$**
Male	15	18	16	17	14
Female	17	12	12	14	13
Total	**32**	**30**	**28**	**31**	**27**

Table 2. Results of Subnetwork Analysis.

Subnetwork	Number of Genes	GO enrichment (OR)
0	91	Peptide cross-linking (30.2), extracellular matrix binding (25.6)
1	82	Myelination (38.6)
2	31	adenylate cyclase-inhibiting GPC AchR signaling pathway (216.6)
3	31	Cell-cell adhesion (84.4)
4	32	Maltose metabolic process (365.64), amino acid transport (123.9)
5	80	TGF beta-activated receptor activity (80.8)
6	5	Lipid transport and binding (Inf)
7	42	G1/S transition of mitotic cell cycle (60.5)
8	59	TLR4 signalling (64.3), TAP binding (50.0)

OR = Odds Ratio

Figure Legends

Figure 1. Generation of BAC transgenic mice expressing wild-type or M337V human TDP-43. (A) Schematic of the human TDP-43-Ypet BAC containing the full length genomic locus of human *TARDBP* engineered with a C-terminal Ypet. A customised integrase system was used to integrate the BAC into the *Rosa26 (Gt(ROSA26)Sor)* genomic locus of mouse ESCs, which ensured stable, single-copy expression of the human protein driven by the endogenous human promotor in the upstream region of the construct. **(B)** Immunoblotting of whole cell lysates from mouse ESCs with a *pan*TDP-43 indicates that human TDP-43 expression levels are considerably below the expression levels of the endogenous mouse Tdp43. **(C)** Antibodies against human-specific TDP-43 and GFP confirm the normal pattern of cellular distribution of human TDP-43 in motor neurons from pre-symptomatic (3 months)

TDP-43$^{WT/-}$ and TDP-43$^{M337V/-}$ mouse spinal cord, which is not observed in NTg controls. Isogenic TDP-43 hemizygous mice express human TDP-43-Ypet across all tissues examined by immunoblotting. **(D)** Human TDP-43-Ypet is expressed at low levels in hemizygous and homozygous cerebral cortex and spinal cord lysates, relative to NTg endogenous Tdp-43, with lower expression relative to endogenous Tdp-43 in spinal cord at this timepoint (3 months) compared to the cerebral cortex (P<0.05, one-way ANOVA with Bonferroni's multiple comparison test). Scale bars: C, 10μm.

Figure 2. TDP-43^{M337V} mice develop age-dependent, progressive weight, survival and motor function deficits. TDP-43^{M337V} mice develop a distinct phenotype compared to nontransgenic (NTg) and TDP-43^{WT} controls. **(A)** Male TDP-43$^{M337V/M337V}$ mice display a slight but statistically significant reduction in weight from 5 months of age (*P<0.05, **P<0.01,
***P<0.001, ****P<0.0001, repeated measures 2way ANOVA/Bonferroni *post hoc* test). **(B)** Female TDP-43$^{M337V/M337V}$ mice show a late deficit in weight compared to controls, starting at 12 months (*P<0.05, repeated measures 2way ANOVA/Bonferroni *post hoc* test). **(C)** Combined data for both sexes indicates a significant survival deficit in TDP-43^{M337V} mice (NTg vs TDP-43$^{M337V/-}$, *P<0.05; NTg vs TDP-43$^{M337V/M337V}$, **P<0.005 median survival 694 days, Mantel-Cox test). **(D)** TDP-43^{M337V} mice displayed a significantly reduced time spent on the accelerating rotarod beginning between the 6 and 9 month timepoints (combined male and female data), compared to NTg controls(**P<0.01, ***P<0.001, ****P<0.0001 repeated measures 2way ANOVA/Bonferroni *post hoc* test). **(E)** TDP-43^{M337V} mice develop progressive grip strength deficits, with combined male and female data from TDP-43$^{M337V/-}$ and TDP-43$^{M337V/M337V}$ mice showing reduced hang time compared to NTg controls (*P<0.05

and ****P<0.0001, repeated measures 2way ANOVA/Bonferroni *post hoc* test). **(F)** In conjunction with motor deficits, total activity of TDP-43$^{M337V/-}$ and TDP-43$^{M337V/M337V}$ mice (combined male and female data) is significantly reduced in open field testing, from 9 months of age (**P<0.01,***P<0.001, ****P<0.001, repeated measures 2way ANOVA/Bonferroni *post hoc* test).

Figure 3. Symptomatic TDP-43^{M337V} mice develop hind-limb lumbrical muscle NMJ deficits. (A) Representative motor endplates from NTg and TDP-43 mice at 9 months of age. NMJs in TDP-43$^{M337V/-}$ and TDP-43$^{M337V/M337V}$ mice have a reduced complexity and size compared to NTg controls. **(B)** From 9 months (*P<0.05, one-way ANOVA with Bonferroni's multiple comparison test) and 12 months (*P<0.05, one-way ANOVA with Bonferroni's multiple comparison test) a significant decrease in post-synaptic area is observed in symptomatic TDP-43$^{M337V/M337V}$ mouse lumbrical muscle compared to NTg controls. **(C)** No significant differences are observed in post-synaptic area in NTg, TDP43$^{WT/WT}$ and TDP-43$^{M337V/M337V}$ gastrocnemius at symptomatic timepoints (P=0.9405, oneway ANOVA with Bonferroni's multiple comparison test). **(D)** Representative lumbrical muscle NMJs from 12 month old NTg and TDP-43-BAC mice analysed for denervation. **(E)** At 12 months there was a significant increase in partially denervated NMJs in the TDP-43$^{M337V/M337V}$ mice compared to NTg controls (*P<0.05, one-way ANOVA with Bonferroni's multiple comparison test). **(F)** Partial denervation was confirmed by the significant loss of synaptic overlap between the axonal immunostaining (2H3/SV2) and that of the endplate (αBTX) only at the 12 month timepoint in TDP-43$^{M337V/M37V}$ mice (*P<0.05, one-way ANOVA with Bonferroni's multiple comparison test). (G) No change in synaptic overlap is observed in the gastrocnemius muscle of TDP-43$^{M337V/M337V}$ mice at 12 months (P=0.5186, one-way ANOVA with Bonferroni's multiple comparison test). Scale bars, 10 μm.

Figure 4. Neuromuscular deficits occur without TDP-43 cytoplasmic mis-localisation, neuronal death or inflammation in symptomatic TDP-43^{M337V} mouse spinal cord. (A) Representative immunohistochemical analysis of 12 month old lumbar spinal cord with *pan*TDP-43 (*top panel*), NeuN (*middle panel*) and Iba1 (*bottom panel*) antibodies displayed no significant qualitative differences between mutant mouse and control spinal cord. Nuclear clearing of TDP-43 or accumulation in the cytoplasm was not observed to be part of the symptomatic phenotype in mutant mice. **(B)** There was no significant change in the number of NeuN-positive neurons in the ventral horn of the lumbar spinal cord in 3 or 12 month old mice, compared to control animals. **(C)** Similarly, no significant change in the number of microglia was observed in presymptomatic or symptomatic mouse lumbar spinal cord. **(D)** No evidence of p62 or phosphorylated TDP-43 is evident in spinal cord from 12 month mice. Scale bars, A, *top and middle panel*, 5 μm; *bottom panel*, 20 μm, D, 5 μm.

Figure 5. Widespread defects in splicing are not part of the pre-symptomatic phase of ALS pathogenesis in TDP-43^{M337V} mice. (A) Principal components analysis shows separation of the TDP-43$^{M337V/-}$ mouse model from NTg and TDP-43$^{WT/-}$ mice along the first principal component. **(B)** Histogram of number of significantly different exon splicing events after permutation of group labels. The red line indicates result obtained with true sample labels. **(C)** Differential expression plotted against mean normalised counts, with all differentially expressed genes coloured in red, shows good normalisation.**(D)** Differential expression between TDP-43$^{M337V/-}$ mutants and TDP-43$^{WT/-}$ /NTg mice was highly robust as demonstrated by random permutation of genotype labels. The red line indicates unpermuted result. **(E)** The 633 differentially expressed genes are functionally related, as demonstrated by Phenotypic Linkage Network Analysis, using a nervous system specific network. The red line

shows the strength of links in the dataset, compared to the distribution of link strength for samples randomly drawn from the nervous system network.

Figure 6. TDP-43^{M337V}-derived primary motor neurons recapitulate TDP-43 cytoplasmic mislocalisation. (A) Under basal conditions (ie, lacking stress) primary motor neurons from TDP-43^{M337V} mice display cytoplasmic mislocalisation of total cellular TDP-43 when stained with a *pan*TDP-43 antibody, compared to NTg and TDP-43^{WT} controls. Importantly, nuclear clearing in mutant-derived primary neurons suggests the mutant form of human TDP-43 can affect the distribution of endogenous mouse TDP-43. **(B)** When quantified, a significantly higher proportion of motor neurons at 7DIV displayed predominantly cytoplasmic TDP-43 in unstressed TDP-43$^{M337V/-}$ cells compared to both NTg and TDP-43^{WT} controls (**P*<0.05, one-way ANOVA with Bonferroni's multiple comparison test). **(C)** Primary motor neurons from TDP-43$^{M337V/-}$ mice have a higher proportion of cells with predominantly cytoplasmic TDP-43 during development in culture, beginning as early as 3DIV (***P*<0.01, unpaired T-test). **(D)** Fluorescence intensity measurements confirm significantly more TDP-43 in the cytoplasmic compartment of TDP-43$^{M337V/-}$ cells, relative to controls (**P*<0.05, one-way ANOVA with Bonferroni's multiple comparison test), **(E)** which is observed as early as 3DIV under basal culture conditions (***P*<0.01, unpaired T-test). **(F)** Immunoblotting of nuclear (N) and cytoplasmic (C) fractions from primary motor neurons at 7DIV confirm accumulation of *pan*TDP-43 levels in the mutant cytoplasmic fraction. **(G)** Immunostaining with anti-GFP identifies significant cytoplasmic mislocalisation of human TDP-43 within TDP-43$^{M337V/-}$ motor neurons compared to TDP-43$^{WT/-}$ controls. **(H)** A significantly higher number of TDP-43$^{M337V/-}$ motor neurons display cytoplasmic mislocalisation of human TDP-43 (**P*<0.05, unpaired T-test), and **(I)** increased fluorescence

intensity of cytoplasmic GFP immunoreactivity in the cytoplasm compared to TDP-43$^{WT/-}$ cells (*P<0.05, unpaired T-test). Scale bars, 5 μm.

Figure 7. TDP-43^{M337V} cytoplasmic mislocalisation is accompanied by altered stress granule dynamics. (A) Representative immunostaining of TIA-1-positive stress granules in primary motor neurons showing increased stress granule formation in response to oxidative stress. **(B)** There is no observable difference in the ability of TDP-43$^{WT/-}$ or NTg primary motor neurons to form TIA-1-, G3BP- or PABP-positive stress granules in response to NaAr exposure. The presence of TDP-43^{M337V} leads to a significant reduction in the number of motor neurons containing stress granules after 60 min exposure to NaAr (*P<0.05, one-way ANOVA with Bonferroni's multiple comparison test). **(C, D)** G3BP-positive stress granules are significantly smaller in TDP-43$^{M337V/-}$ motor neurons (C; ***P<0.0001), with a shift towards the left when granule area is plotted as a frequency distribution (D). **(E, F)** A similar reduction in granule area is observed for PABP-positive granules in TDP-43$^{M337V/-}$ motor neurons **(**E, *P<0.05, unpaired t-test), with a shift to smaller stress granule in a frequency distribution (F). **(G)** Mutant human TDP-43 shows reduced recruitment to stress granules. Co-localisation between GFP and TIA-1 is significantly reduced in the cytoplasm of TDP43^{M337V} motor neurons compared to TDP-43^{WT} controls (*P<0.05 each timepoint, unpaired ttest). **(H)** Following removal of sodium arsenite, and subsequent recovery from oxidative stress, the proportion of TDP-43$^{M337V/-}$ motor neurons producing stress granules quickly returned to control proportions, suggesting possible impairment in stress granule primary aggregation (*P<0.05, unpaired t-test). **(I)** TDP-43$^{M337V/-}$ motor neurons display reduced survival 3 hours after NaAr exposure at 7DIV compared to controls (*P<0.05, one-way

ANOVA with Bonferroni's multiple comparison test). **(J, K)** The presence of TDP-43^{M337V} leads to a significant reduction in the proportion of motor neurons containing G3BP and PABP-positive stress granules after 60 min exposure to NaAr (*P<0.05, one-way ANOVA with Bonferroni's multiple comparison test). **(L)** TDP-43$^{M337V/-}$ ESC-motor neurons display significantly reduced numbers of both G3BP- and PABP-positive stress granules/cell following 60 min exposure to NaAr (**P<0.01, ***P<0.001, one-way ANOVA with Bonferroni's multiple comparison test). **(M)** TDP-43$^{M337V/-}$ ESC-motor neurons display reduced survival 3 hours after NaAr exposure at 2DIV compared to controls (*P<0.05, oneway ANOVA with Bonferroni's multiple comparison test). Scale bars, 5 μm.

Supplementary figures

Supplementary Figure 1. Male and female mice TDP-43^{M337V} mice develop agedependent, progressive survival and motor function deficits. (A) Male TDP-43$^{M337V/-}$ mice display reduced survival compared to NTg controls (*P<0.05, Mantel-Cox test), though TDP-43^{M337V} homozygote survival reduction did not reach significance (Mantel-Cox test). **(B)** Female TDP-43^{M337V} mice have reduced survival in the second year (NTg vs TDP43$^{M337V/-}$, *P<0.05, median survival 703.5 days; NTg vs TDP-43$^{M337V/M337V}$, *P<0.05, median survival 544 days, Mantel-Cox test). **(C)** Male TDP-43^{M337V} mice displayed a significantly reduced time spent on the accelerating rotarod beginning between the 6 and 9 month timepoints (NTg vs TDP-43^{M337V}, *P<0.05, ***P<0.001, ****P<0.0001 repeated measures 2way ANOVA/Bonferroni *post hoc* test**. (D)** Female TDP-43$^{M337V/-}$and TDP-43$^{M337V/M337V}$ mice displayed a similar progressive motor function deficit on the accelerating rotarod beginning between the 9 and 12 timepoint timepoints, compared to NTg and TDP-43^{WT} controls (*P<0.05, **P<0.01, ****P<0.01, repeated measures 2way

ANOVA/Bonferroni *post hoc* test). **(E)** Male TDP-43$^{M337V/-}$ and TDP-43$^{M337V/M337V}$ mice display reduced hang time compared to NTg controls (**P<0.01, ***P<0.001 and ****P<0.0001, repeated measures 2way ANOVA/Bonferroni *post hoc* test). **(F)** Female TDP-43$^{M337V/-}$ and TDP43$^{M337V/M337V}$ mice display a similarly progressive grip strength reduction between 6-9 months (*P<0.01, ***P<0.001 ****P<0.0001, repeated measures 2way ANOVA/Bonferroni *post hoc* test). **(G)** Total activity of male TDP-43$^{M337V/M337V}$ mice is significantly reduced in open field testing at 9 months of age (**P<0.01, repeated measures 2way

ANOVA/Bonferroni *post hoc* test). (H) Similarly, female TDP-43 TDP-43$^{M337V/M337V}$ mice display significantly activity in open field testing at 12 months (***P<0.001, repeated measures 2way ANOVA/Bonferroni *post hoc* test).

Supplementary Figure 2. Weight had no effect on the progressive reduction in grip strength observed in TDP-43M337V mice. (A) Holding impulse (weight × hang time) is progressively reduced for male TDP-43^{M337V} mice from 6 months of age, compared to NTg controls (**P<0.01, ***P<0.001 and ****P<0.0001, repeated measures 2way ANOVA/Bonferroni *post hoc* test**). (B)** Female mutant mice display similar reductions in holding impulse from 9 months of age (*P<0.05, **P<0.01 and ***P<0.001, repeated measures 2way ANOVA/Bonferroni *post hoc* test). (C) Combined data for both male and female shows a progressive reduction in holding impulse in TDP-43^{M337V} mice (**P<0.01 and ****P<0.0001).

Supplementary Figure 3. Neuromuscular deficits occur without TDP-43 cytoplasmic mis-localisation or protein aggregation in 24 month, symptomatic TDP-43^{M337V} mouse spinal cord. (A) Immunostaining of lumbar spinal cord was carried out with anti-GFP to identify human TDP-43. Ventral horn motor neurons in NTg controls were negative for GFP immunoreactivity, as expected. Representative GFP immunoreactivy is shown from TDP43$^{WT/WT}$ and TDP-43$^{M337V/M337V}$ mice. **(B)** No significant difference in the proportion of ventral horn motor neuorns (n=3, ≥10 cells per mouse) with cytoplasmic mislocalisation of GFP was observed in TDP-43$^{M337V/M337V}$ mice compared to TDP-43$^{WT/WT}$ controls. No significant difference was observed in the fluorescence intensity of cytoplasmic GFP compared to nuclear GFP in TDP-43$^{M337V/M337V}$ mice compared to TDP-43$^{WT/WT}$ controls. Scale bars, NTg, 5 μm, TDP-43$^{WT/WT}$ and TDP-43$^{M337V/M337V}$, 10 μm.

Supplementary Figure 4. Human TDP-43 protein levels are elevated in the brain of presymptomatic TDP-43^{M337V} homozygous mice without disease pathology.

(A) Immunoblotting of soluble and insoluble lysates from the CNS of pre-symptomatic 3 month old mice with a *pan*TDP-43 antibody indicates that **(B)** human TDP-43-Ypet is significantly elevated in the insoluble fraction from homozygous TDP-43^{M337V} brain versus hemizygous TDP-43$^{WT/-}$ (*P<0.05, one-way ANOVA with Bonferroni's multiple comparison test). **(C)** In spinal cord from 3 month old mice there is a trend towards elevated human TDP43 protein in TDP-43$^{M337V/-}$ and TDP-43$^{M337V/M337V}$ mice but significance is not reached at this timepoint.

Supplementary Figure 5. Human TDP-43 protein levels are elevated in the brain and spinal cord of symptomatic TDP-43^{M337V} mice. (A) Immunoblot of soluble and insoluble CNS lysates from 9 month old TDP-43 mice. **(B, C)** Human TDP-43-Ypet protein levels are elevated in both the soluble and insoluble protein fractions of brain (B) and spinal cord (C) at 9 months (**P* and ***P*<0.05, one-way ANOVA with Bonferroni's multiple comparison test).

Supplementary Figure 6. Human TDP-43 mRNA expression in TDP-43^{M337V} CNS tissue. (A, B) Human TDP-43 mRNA levels are elevated in TDP-43$^{WT/WT}$ and TDP43$^{M337V/M337V}$ cortex and lumbar spinal cord in pre-symptomatic (3 month) mice, compared to hemizygously expressing mice. By 9 months of age, human TDP-43 mRNA levels are comparable across all mouse lines in the symptomatic cerebral cortex and spinal cord (**P* and ***P*<0.05, one-way ANOVA with Bonferroni's multiple comparison test).

Supplementary Figure 7. Primary and ESC-derived motor neurons express motor neuron markers. (A) Primary motor neurons from each line identified with the motor neuron marker SMI-32. TDP-43 is predominantly nuclear in NTg and TDP-43$^{WT/-}$ cells, but displays significantly increased TDP-43 in the cytoplasmic compartment of TDP-43$^{M337V/-}$ cells. The nucleus has been highlighted artificially in the first column (yellow line). **(B)** ESC-derived motor neurons were counterstained with βIII-tubulin and a battery of motor neuron-specific markers. Overlap immunostaining indicates that the majority of βIII-tubulin positive cells from each line express SMI-32, Islet-1 and ChAT, while Hb9 appears down-regulated as cells mature. Scale bars A, 5 μm; B 10 μm.

Supplementary Figure 8. TDP-43$^{M337V/-}$-derived cortical neurons fail to recapitulate key phenotypic characteristics. (A) Cultured cortical neurons from TDP-43$^{M337V/-}$ mice do not display significant cytoplasmic mislocalisation of TDP-43 compared to NTg controls. **(B)** When quantified, there is no significant difference in the proportion of cortical neurons displaying TDP-43 cytoplasmic mislocalisation (P=0.8308, one-way ANOVA with Bonferroni's multiple comparison test). **(C)** No increase is observed in the levels of TDP-43 in the cytoplasmic compartment of TDP-43$^{M337V/-}$ cells, relative to NTg controls (P= 0.1247, unpaired T-test). **(D, E)** The presence of mutant human TDP-43 does not lead to an altered stress granule response in cortical neurons in response to increasing oxidative stress. **(F)** Significant survival deficits are evident in mutant-derived cortical neurons at 10DIV, independent of stress induction (*P<0.05, one-way ANOVA with Bonferroni's multiple comparison test). Scale bars A, 5 µm; D 5 µm.

Supplementary Figure 9. Western blots from Figure 1.

Supplementary Figure 10. Western blots from Figure 2.

Supplementary Figure 11. Western blots from Figure 6.

Supplementary Figure 12. Western blots from Supplementary Figure 5.

Figures

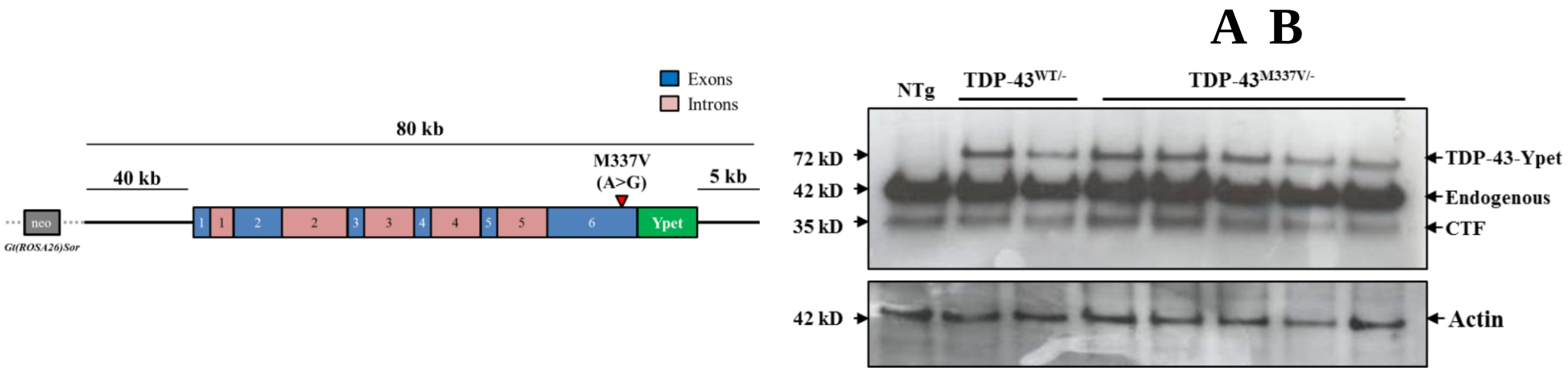

Fig. 1

A

C TDP-43WT/- TDP-43M337V/- NTg

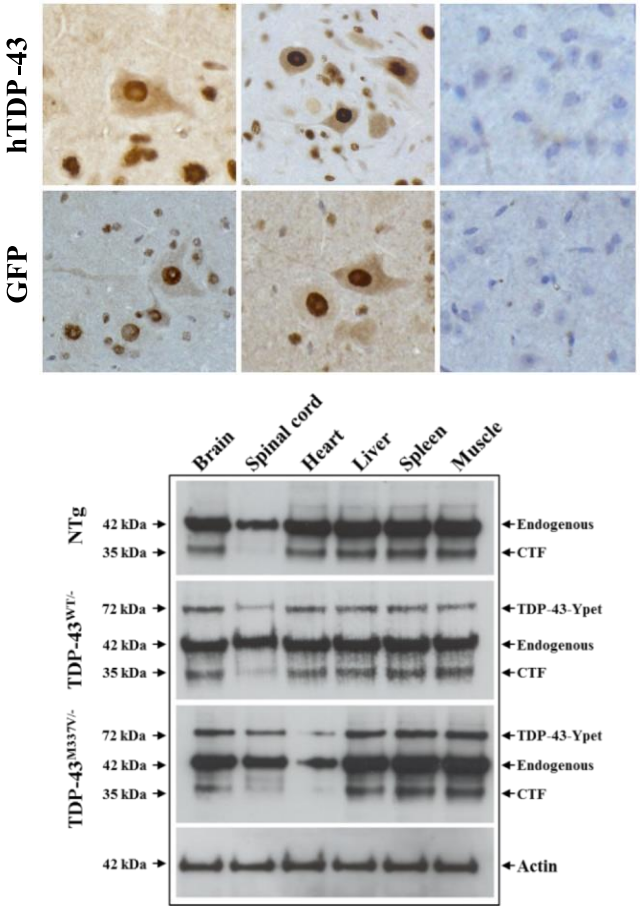

D

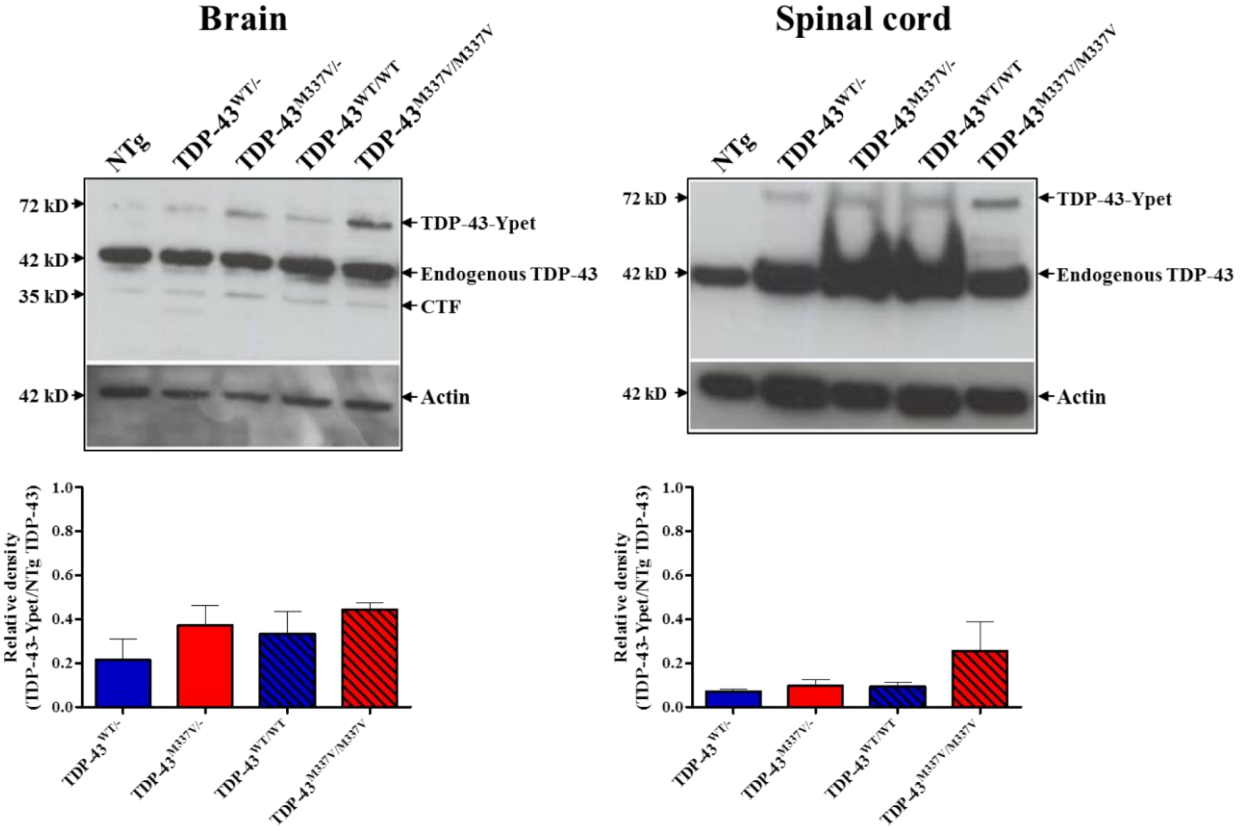

Fig. 2

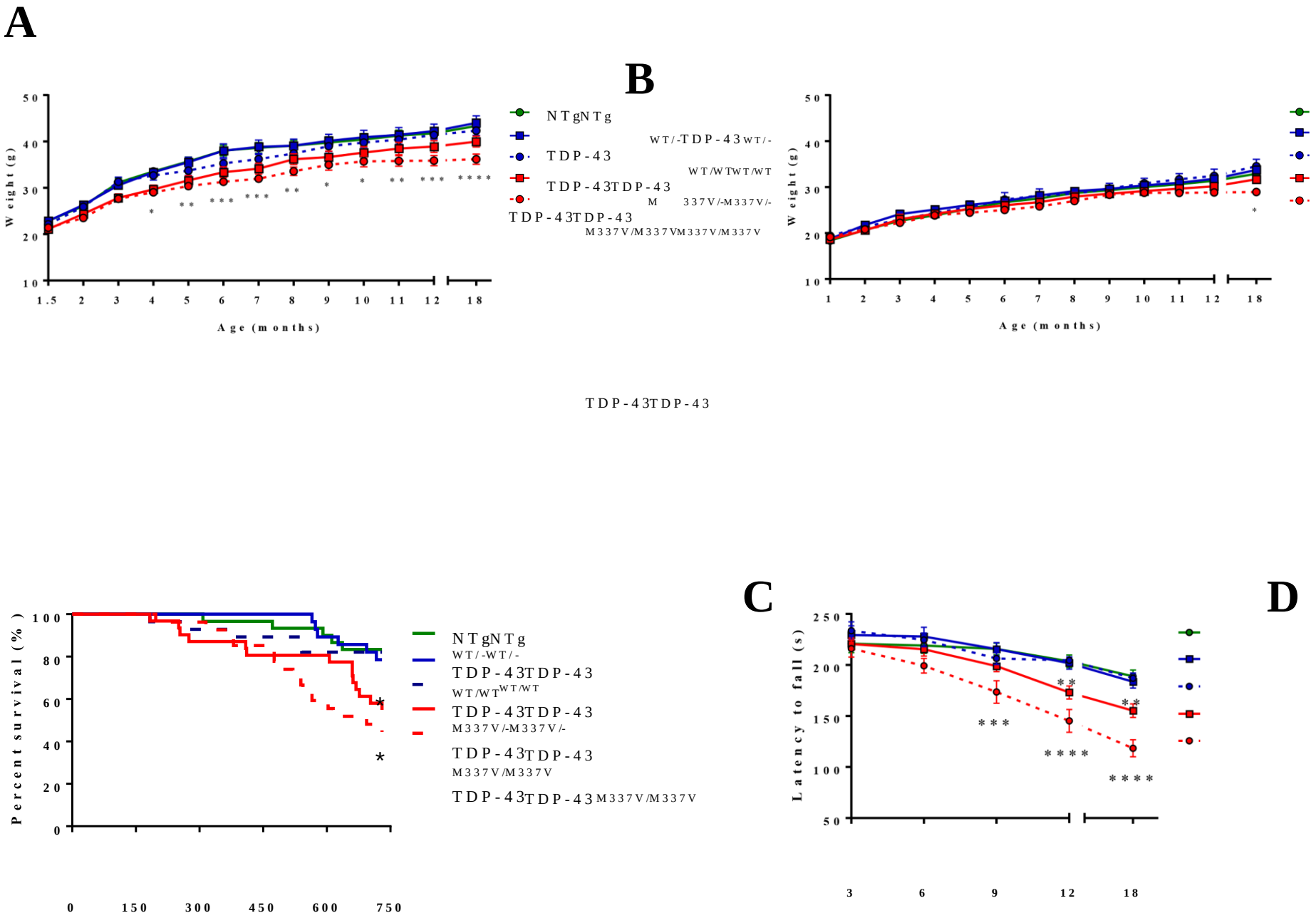
A
B
C
D
Weight (g)
Age (months)
NTgNTg
WT/-TDP-43WT/-
TDP-43WT/WTWT/WT
TDP-43TDP-43M337V/-M337V/-
TDP-43TDP-43M337V/M337VM337V/M337V
TDP-43TDP-43
Percent survival (%)
NTgNTg WT/-WT/-
TDP-43TDP-43 WT/WTWT/WT
TDP-43TDP-43 M337V/-M337V/-
TDP-43TDP-43 M337V/M337V
TDP-43TDP-43M337V/M337V
Latency to fall (s)

Fig. 3

A

E

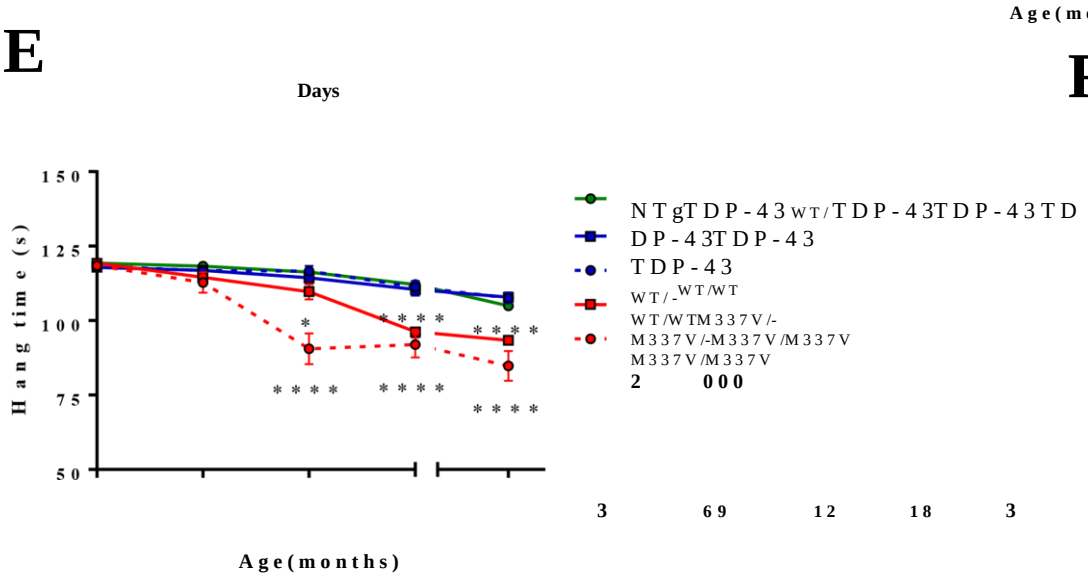
Days
Hang time (s)
150
125
100
75
50
Age(months)
3
6
9
12
18
NTgTDP-43WT/TDP-43TDP-43TD
DP-43TDP-43
TDP-43
WT/-WT/WT
WT/WTM337V/-
M337V/-M337V/M337V
M337V/M337V
2000

F

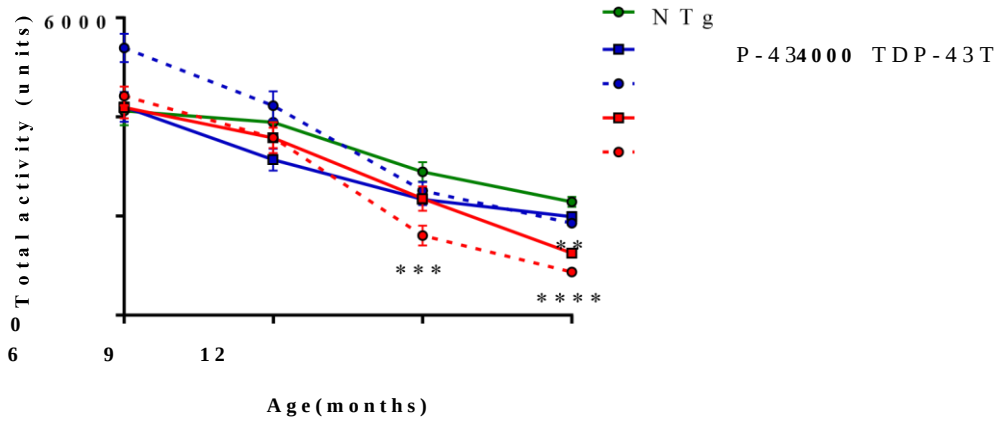
Age(months)
Total activity (units)
6000
0
3
6
9
12
Age(months)
NTg
P-434000 TDP-43T

Fig. 4

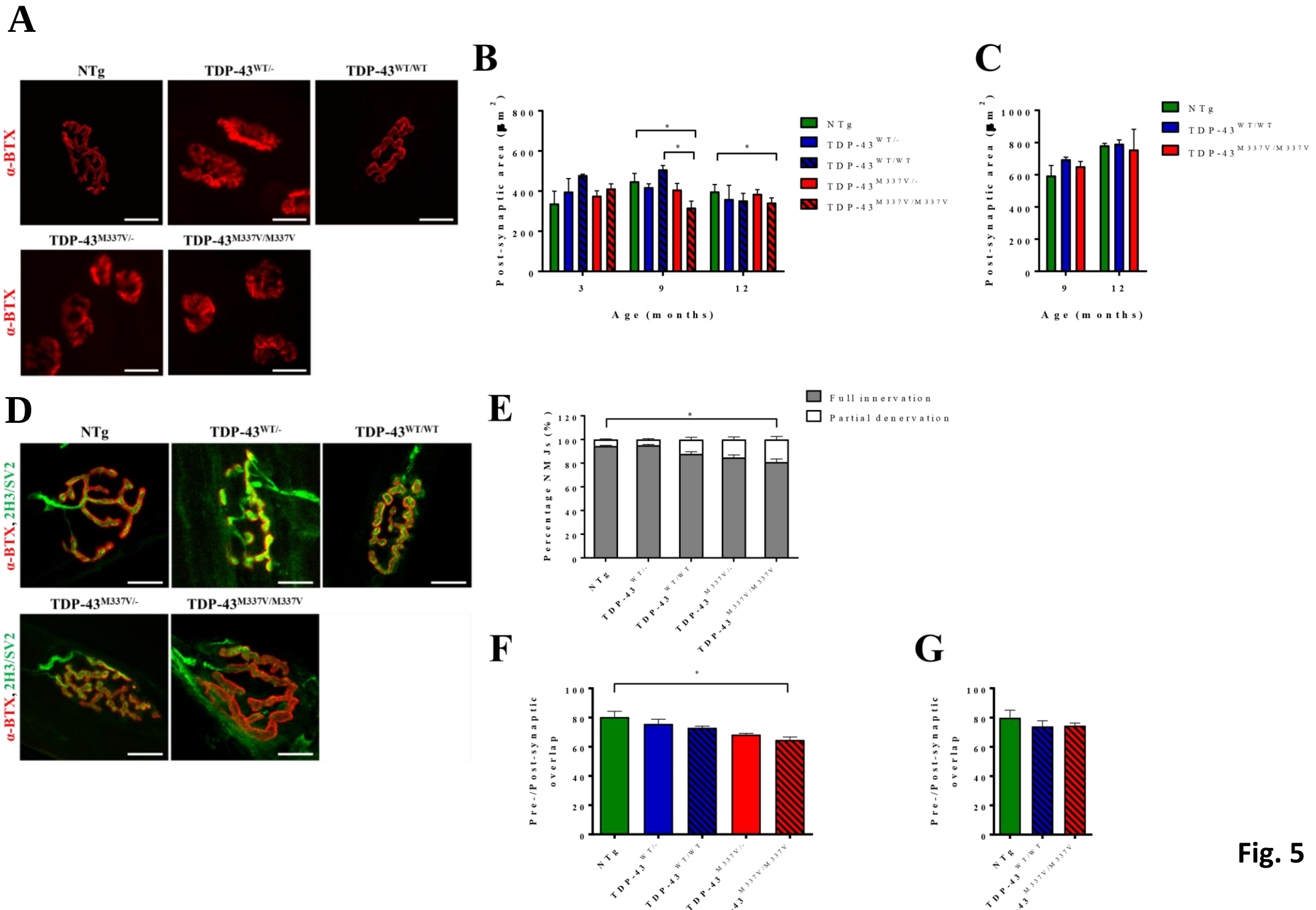
A
NTg
TDP-43WT/-
TDP-43WT/WT
α-BTX
TDP-43M337V/-
TDP-43M337V/M337V
α-BTX
B
Post-synaptic area (μm2)
800
600
400
200
0
3
9
12
Age (months)
NTg
TDP-43WT/-
TDP-43WT/WT
TDP-43M337V/-
TDP-43M337V/M337V
C
Post-synaptic area (μm2)
1000
800
600
400
200
0
9
12
Age (months)
NTg
TDP-43WT/WT
TDP-43M337V/M337V
D
NTg
TDP-43WT/-
TDP-43WT/WT
α-BTX, 2H3/SV2
TDP-43M337V/-
TDP-43M337V/M337V
α-BTX, 2H3/SV2
E
Percentage NMJs (%)
120
100
80
60
40
20
0
Full innervation
Partial denervation
NTg
TDP-43WT/-
TDP-43WT/WT
TDP-43M337V/-
TDP-43M337V/M337V
F
Pre-/Post-synaptic overlap
100
80
60
40
20
0
NTg
TDP-43WT/-
TDP-43WT/WT
TDP-43M337V/-
TDP-43M337V/M337V
G
Pre-/Post-synaptic overlap
100
80
60
40
20
0
NTg
TDP-43WT/WT
TDP-43M337V/M337V

Fig. 5

A

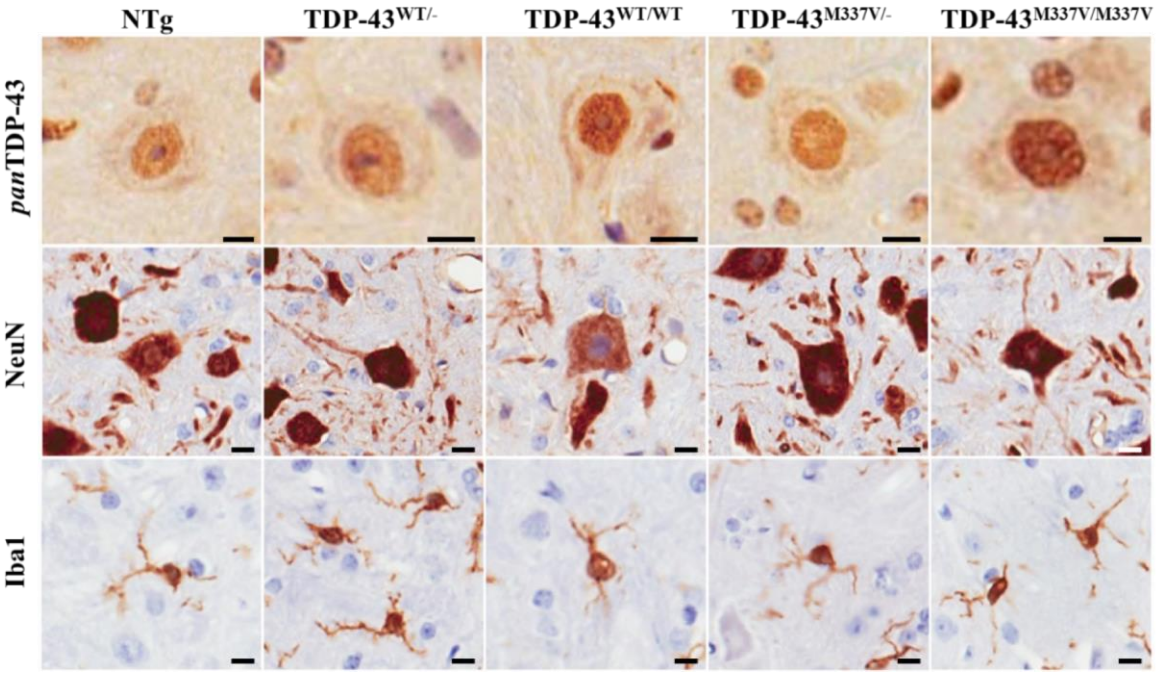
NTg
TDP-43WT/-
TDP-43WT/WT
TDP-43M337V/-
TDP-43M337V/M337V
panTDP-43
NeuN
Iba1

B

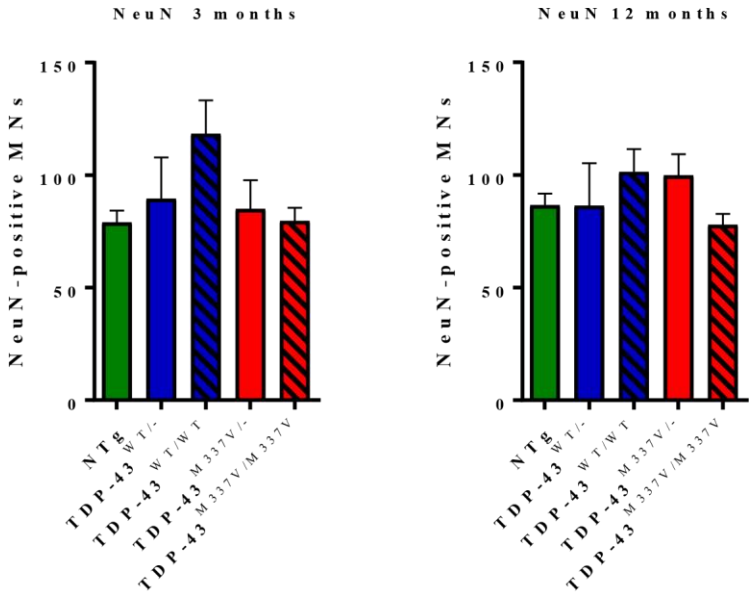
NeuN 3 months
NeuN 12 months
NeuN-positive MNs
150
100
50
0
NTg
TDP-43WT/-
TDP-43WT/WT
TDP-43M337V/-
TDP-43M337V/M337V

Fig. 6

A

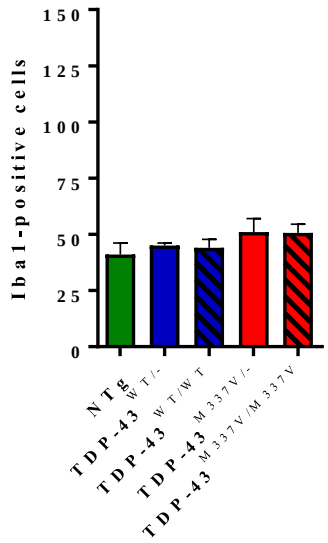
Iba1-positive cells
150
125
100
75
50
25
0
NTg
TDP-43 WT/-
TDP-43 WT/WT
TDP-43 M337V/-
TDP-43 M337V/M337V

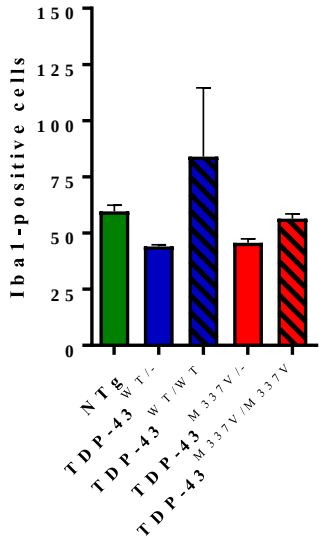
Iba1-positive cells
150
125
100
75
50
25
0
NTg
TDP-43 WT/-
TDP-43 WT/WT
TDP-43 M337V/-
TDP-43 M337V/M337V

C **D**

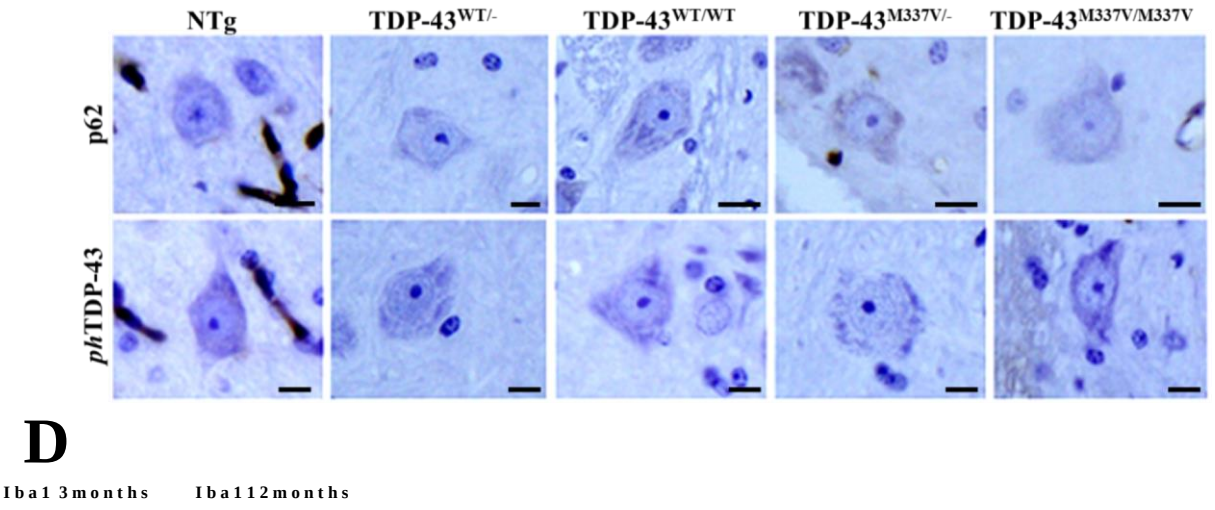
NTg
TDP-43WT/-
TDP-43WT/WT
TDP-43M337V/-
TDP-43M337V/M337V
p62
phTDP-43
Iba1 3months
Iba1 12months

Fig. 7

ABC

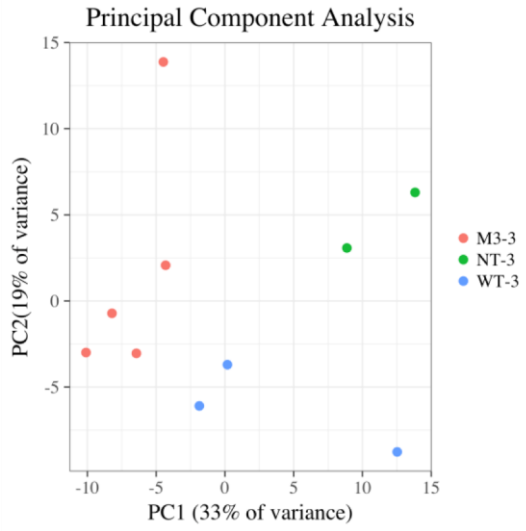
Principal Component Analysis
PC2(19% of variance)
PC1 (33% of variance)
M3-3
NT-3
WT-3

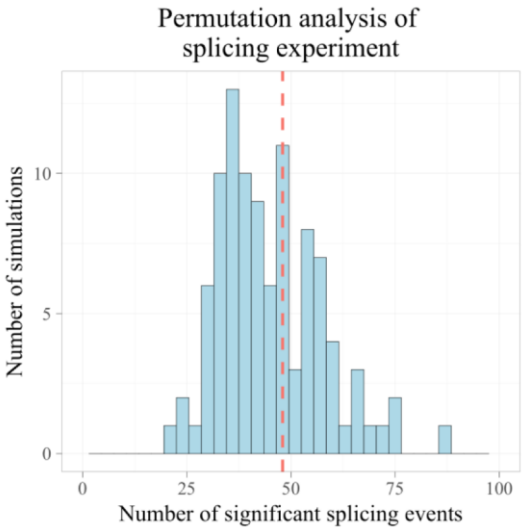
Permutation analysis of splicing experiment
Number of simulations
Number of significant splicing events

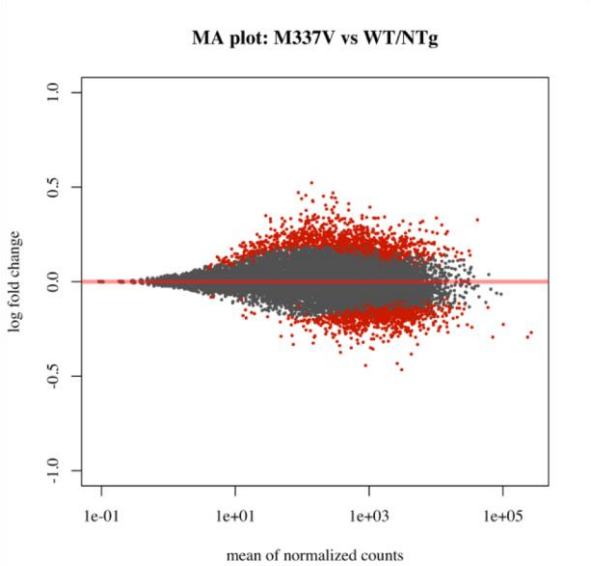
MA plot: M337V vs WT/NTg
log fold change
mean of normalized counts

D

E

Fig. 8

A

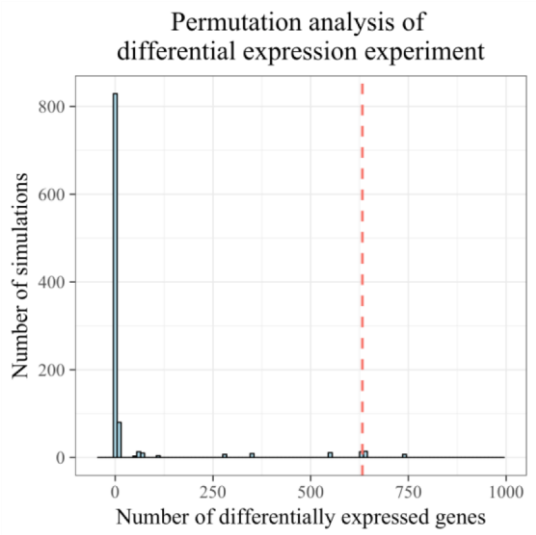
Permutation analysis of
differential expression experiment
Number of simulations
0
200
400
600
800
0
250
500
750
1000
Number of differentially expressed genes

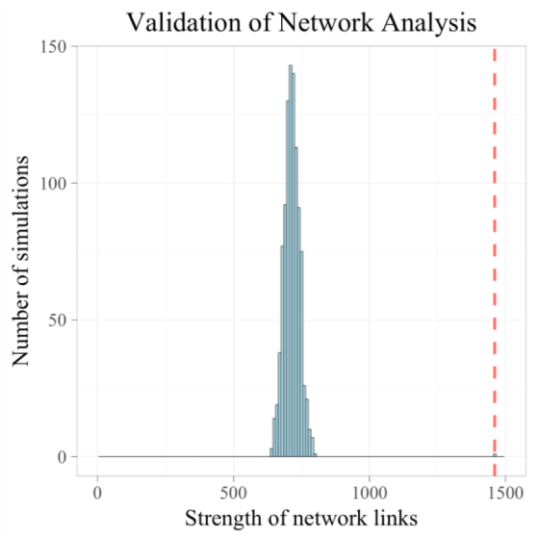
Validation of Network Analysis
Number of simulations
0
50
100
150
0
500
1000
1500
Strength of network links

Fig. 9

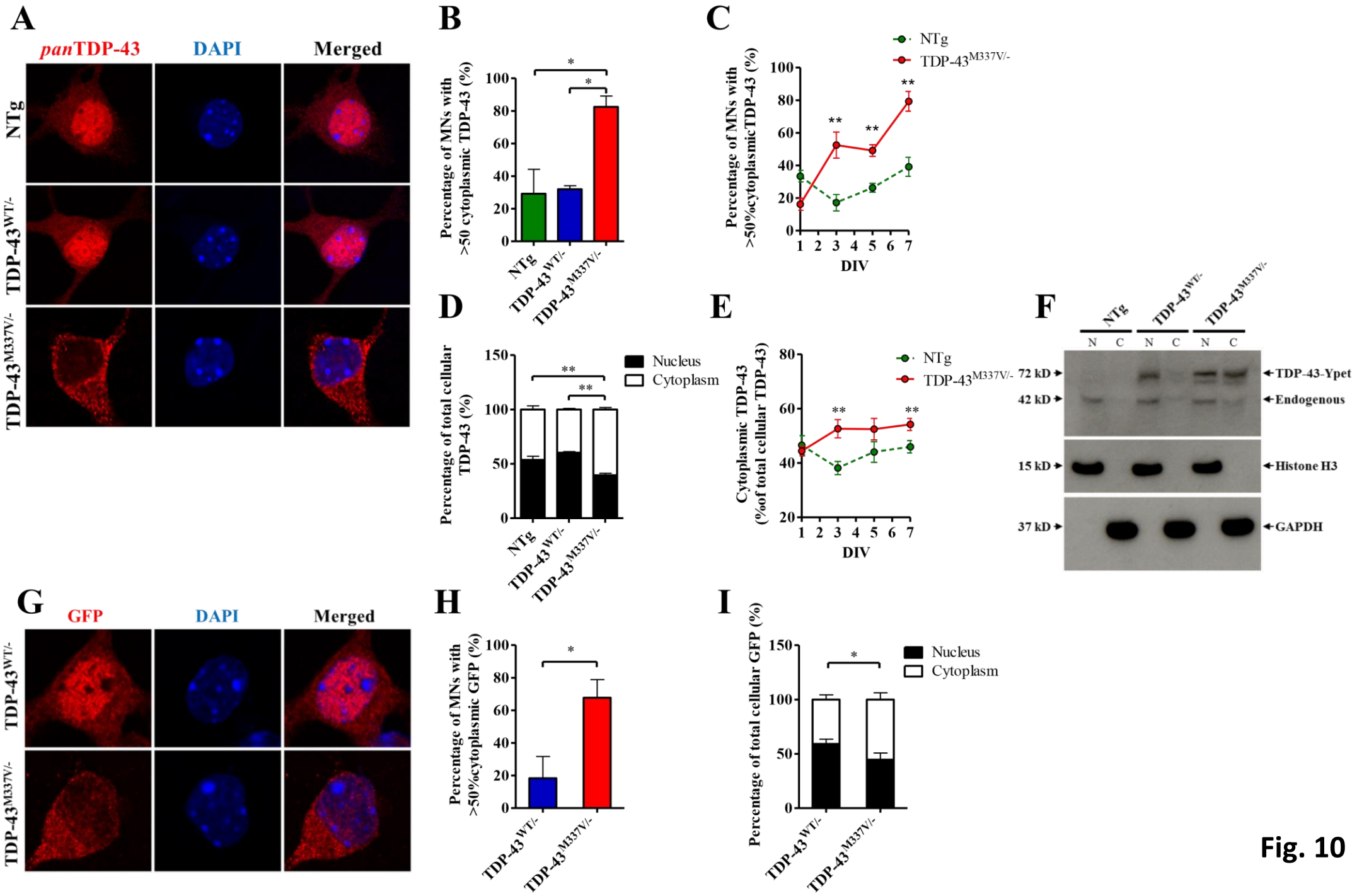
A
panTDP-43
DAPI
Merged
NTg
TDP-43WT/-
TDP-43M337V/-
B
Percentage of MNs with >50 cytoplasmic TDP-43 (%)
NTg
TDP-43WT/-
TDP-43M337V/-
C
NTg
TDP-43M337V/-
Percentage of MNs with >50%cytoplasmicTDP-43 (%)
DIV
D
Nucleus
Cytoplasm
Percentage of total cellular TDP-43 (%)
E
NTg
TDP-43M337V/-
Cytoplasmic TDP-43 (%of total cellular TDP-43)
DIV
F
NTg
TDP-43WT/-
TDP-43M337V/-
N C N C N C
72 kD
42 kD
TDP-43-Ypet
Endogenous
15 kD
Histone H3
37 kD
GAPDH
G
GFP
DAPI
Merged
TDP-43WT/-
TDP-43M337V/-
H
Percentage of MNs with >50%cytoplasmic GFP (%)
I
Nucleus
Cytoplasm
Percentage of total cellular GFP (%)

Fig. 10

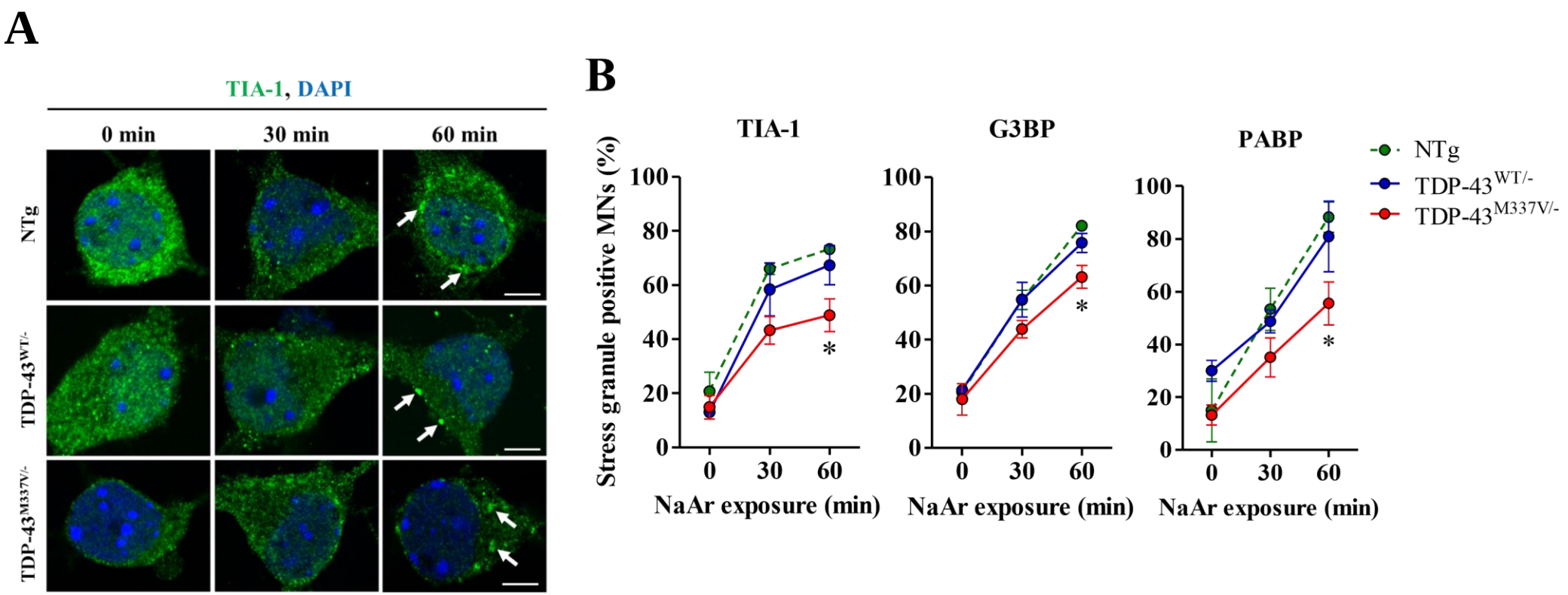
A
TIA-1, DAPI
0 min
30 min
60 min
NTg
TDP-43WT/-
TDP-43M337V/-
B
TIA-1
G3BP
PABP
Stress granule positive MNs (%)
NaAr exposure (min)
NTg
TDP-43WT/-
TDP-43M337V/-

Fig. 11

C

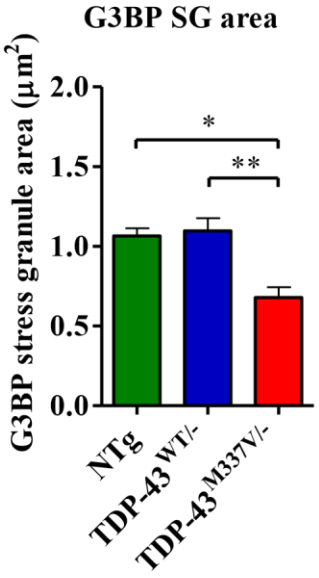
G3BP SG area
G3BP stress granule area (µm²)
2.0
1.5
1.0
0.5
0.0
*
**
NTg
TDP-43 WT/-
TDP-43 M337V/-

D

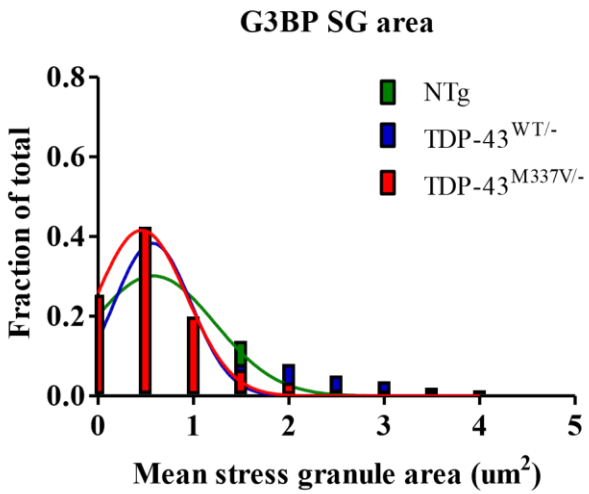
G3BP SG area
Fraction of total
0.8
0.6
0.4
0.2
0.0
0
1
2
3
4
5
Mean stress granule area (um²)
NTg
TDP-43 WT/-
TDP-43 M337V/-

E

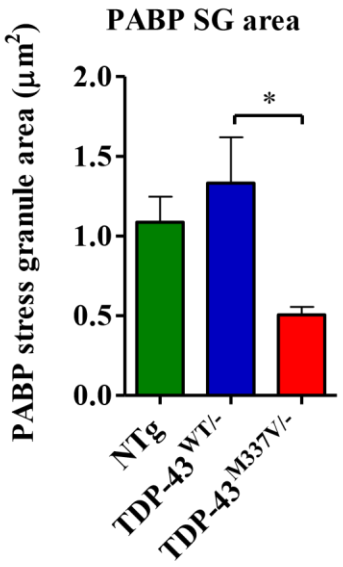
PABP SG area
PABP stress granule area (µm²)
2.0
1.5
1.0
0.5
0.0
*
NTg
TDP-43 WT/-
TDP-43 M337V/-

F

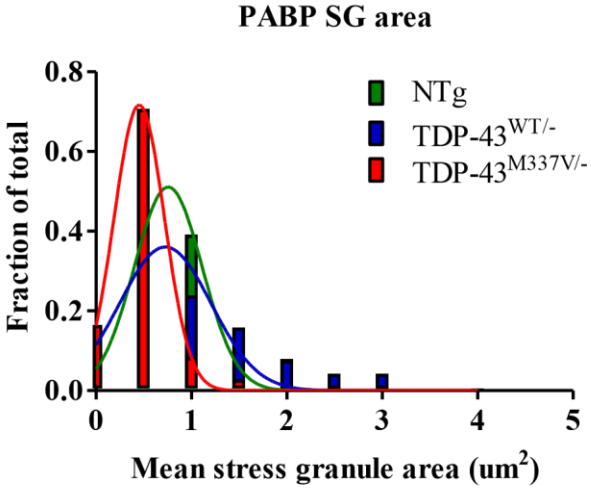
PABP SG area
Fraction of total
0.8
0.6
0.4
0.2
0.0
0
1
2
3
4
5
Mean stress granule area (um²)
NTg
TDP-43 WT/-
TDP-43 M337V/-

Fig. 12

G **Co-localisation: GFP and TIA-1**

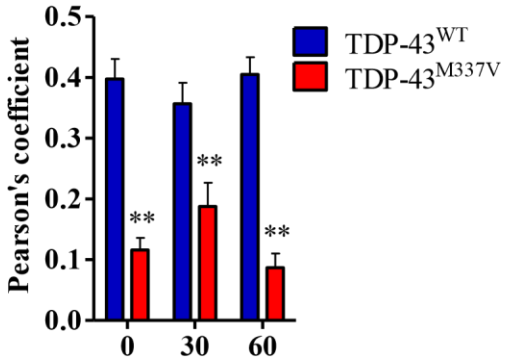

NaAr exposure (min)

H

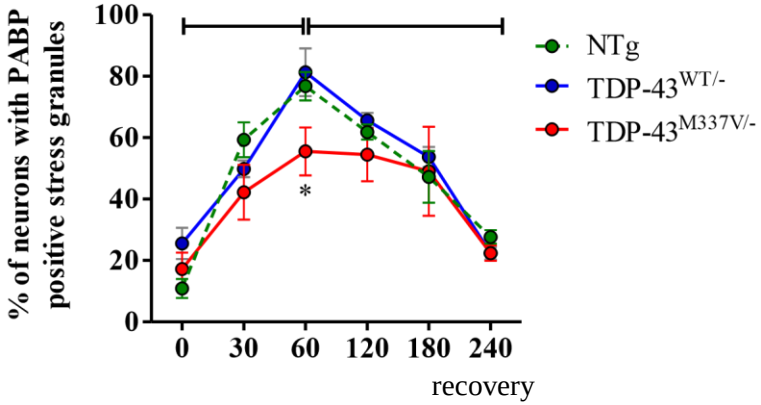

Time (min)

I

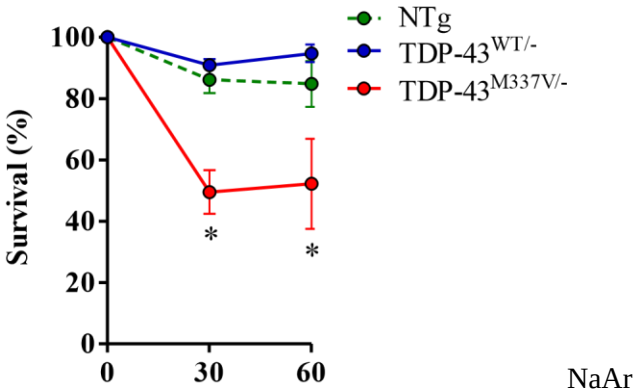

NaAr exposure (min)

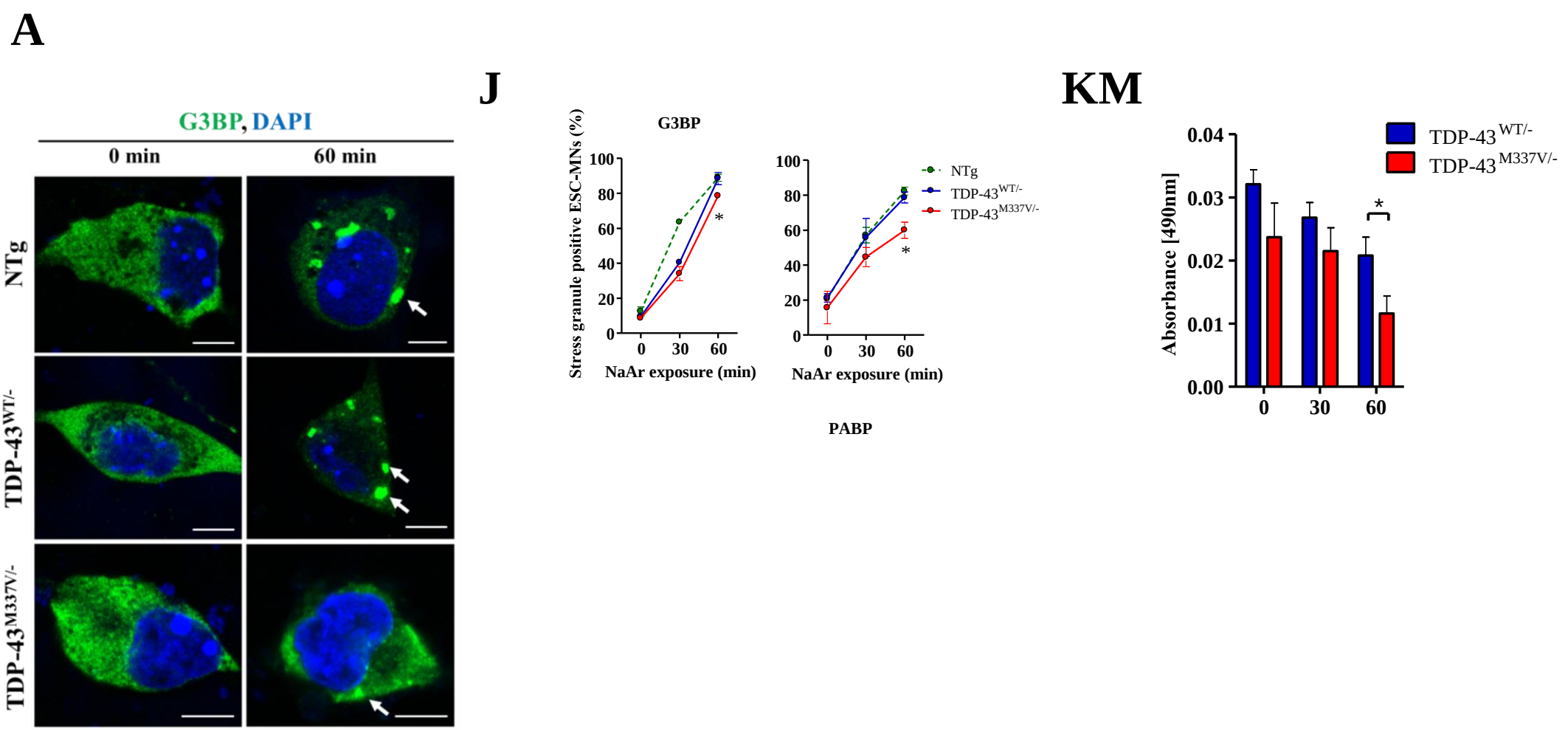
A
G3BP, DAPI
0 min
60 min
NTg
TDP-43WT/-
TDP-43M337V/-
J
G3BP
PABP
Stress granule positive ESC-MNs (%)
NaAr exposure (min)
NaAr exposure (min)
NTg
TDP-43WT/-
TDP-43M337V/-
KM
Absorbance [490nm]
TDP-43WT/-
TDP-43M337V/-

A

L

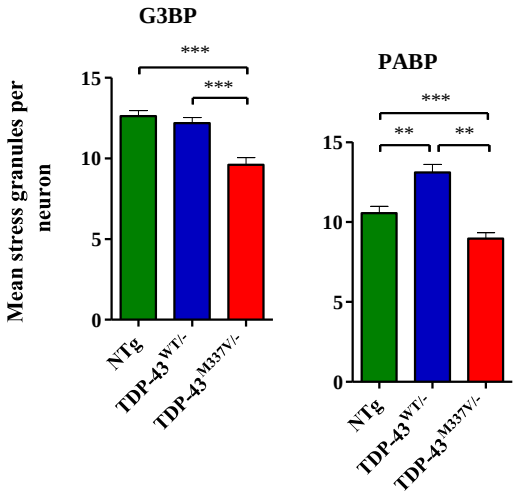

NaAr exposure (min)

Fig. 7

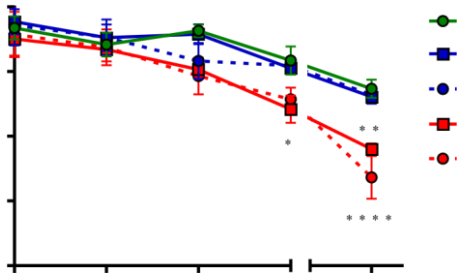

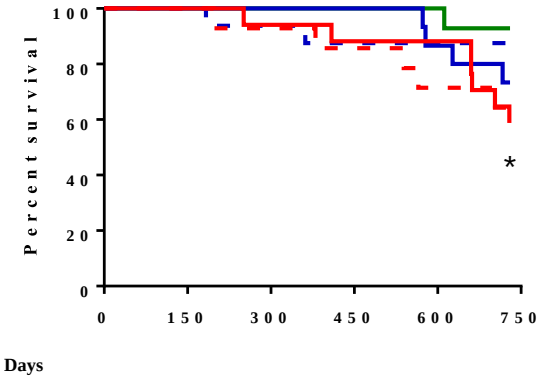

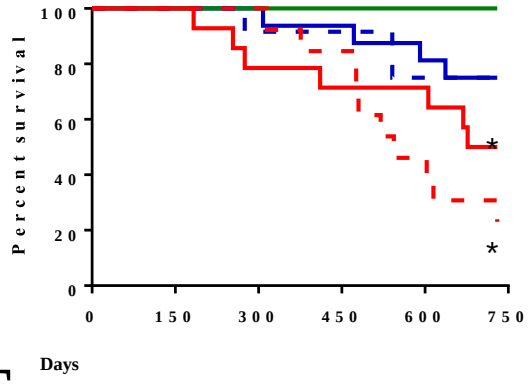

E

D

Rotarod - Female

250NTg

B

Survival - Female

Supp. Fig. 2

A

Grip strength - Male

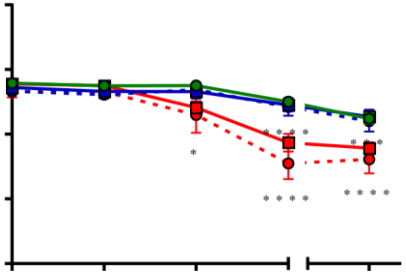

C

Rotarod - Male

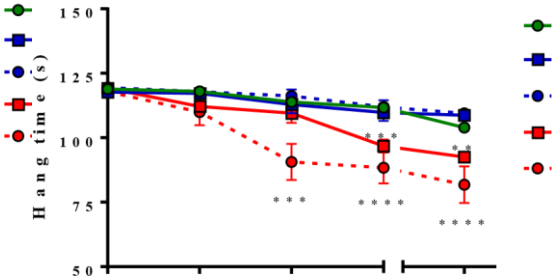

F

Grip strength - Female

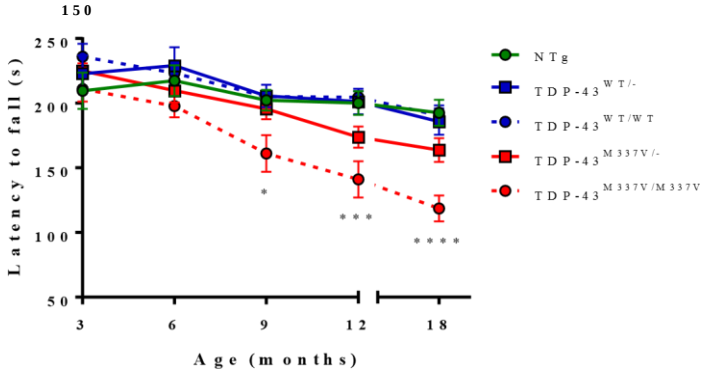

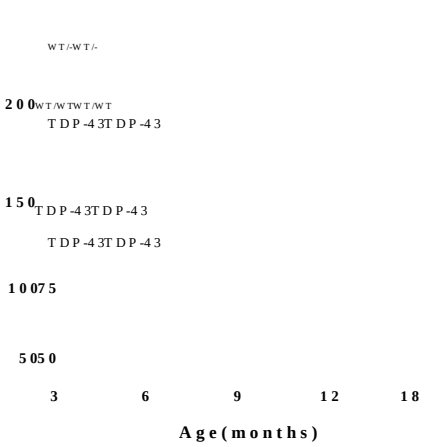

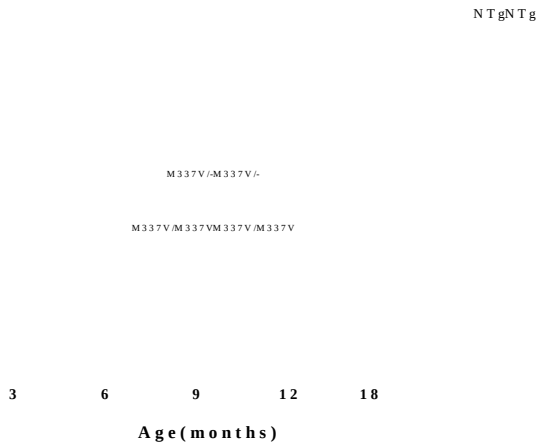

A

G Open field - Male

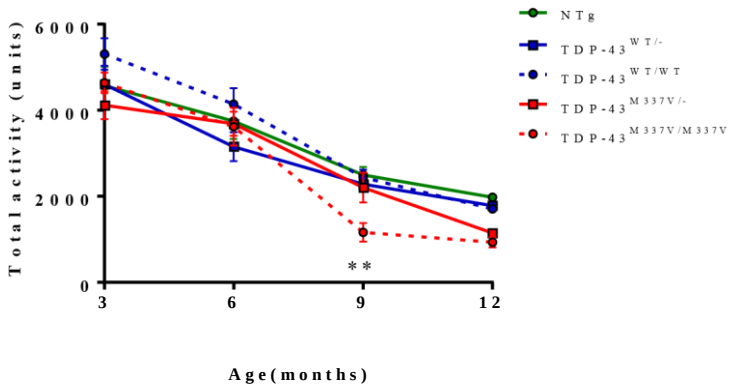

H Open field - Female

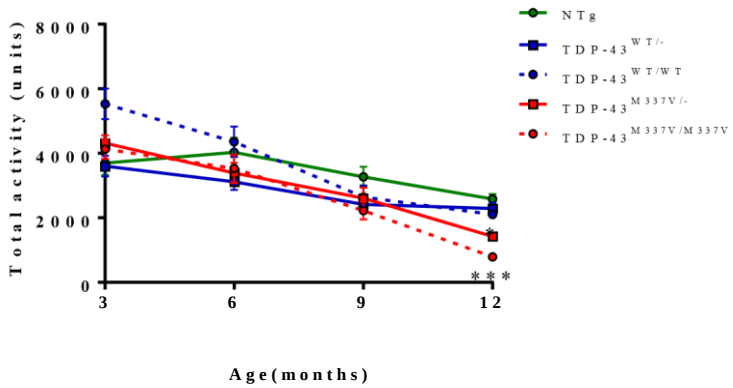

Supp. Fig. 1

Holding impulse - Male

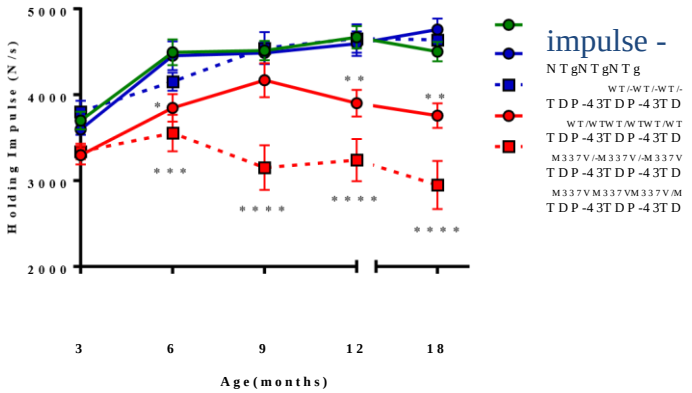

B Holding impulse - Female

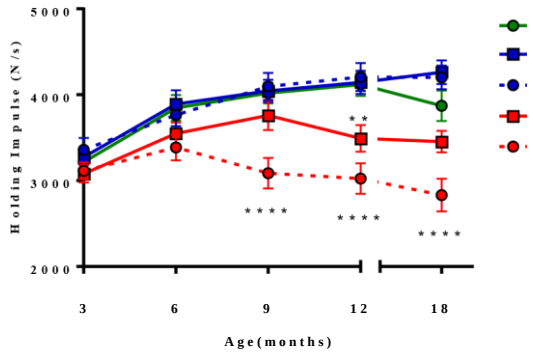

C Holding

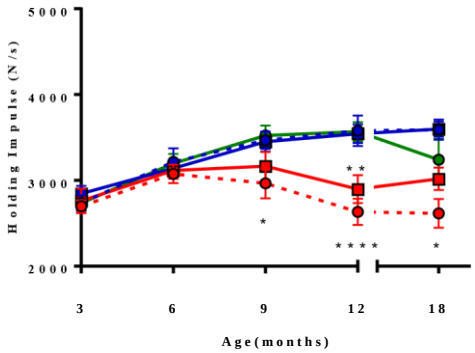

Sup

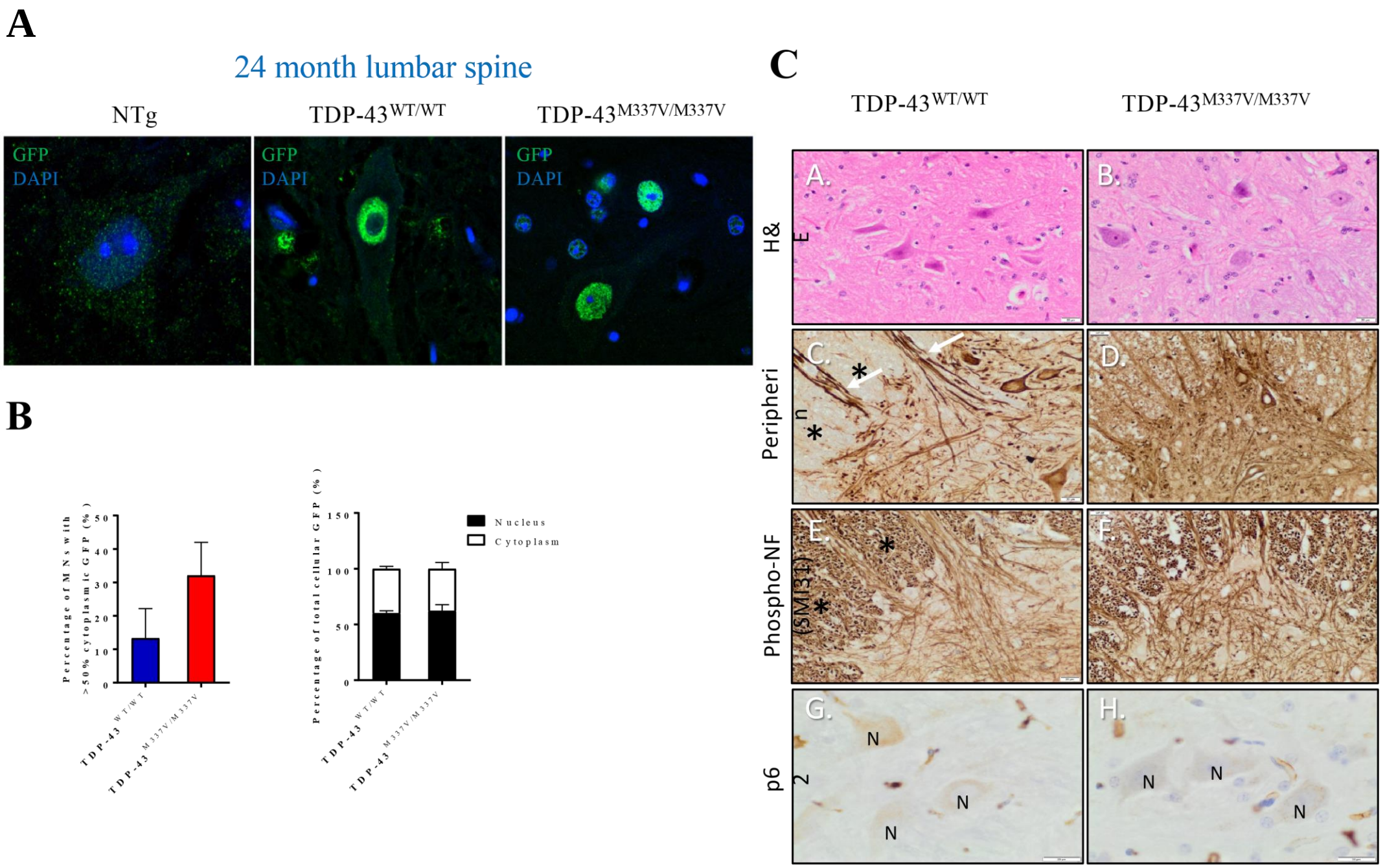
A
24 month lumbar spine
NTg
TDP-43WT/WT
TDP-43M337V/M337V
GFP
DAPI
B
Percentage of MNs with >50% cytoplasmic GFP (%)
TDP-43 WT/WT
TDP-43 M337V/M337V
Percentage of total cellular GFP (%)
Nucleus
Cytoplasm
C
TDP-43WT/WT
TDP-43M337V/M337V
H&E
Peripherin
Phospho-NF (SMI31)
p62
A.
B.
C.
D.
E.
F.
G.
H.
N

Supp. Fig. 3

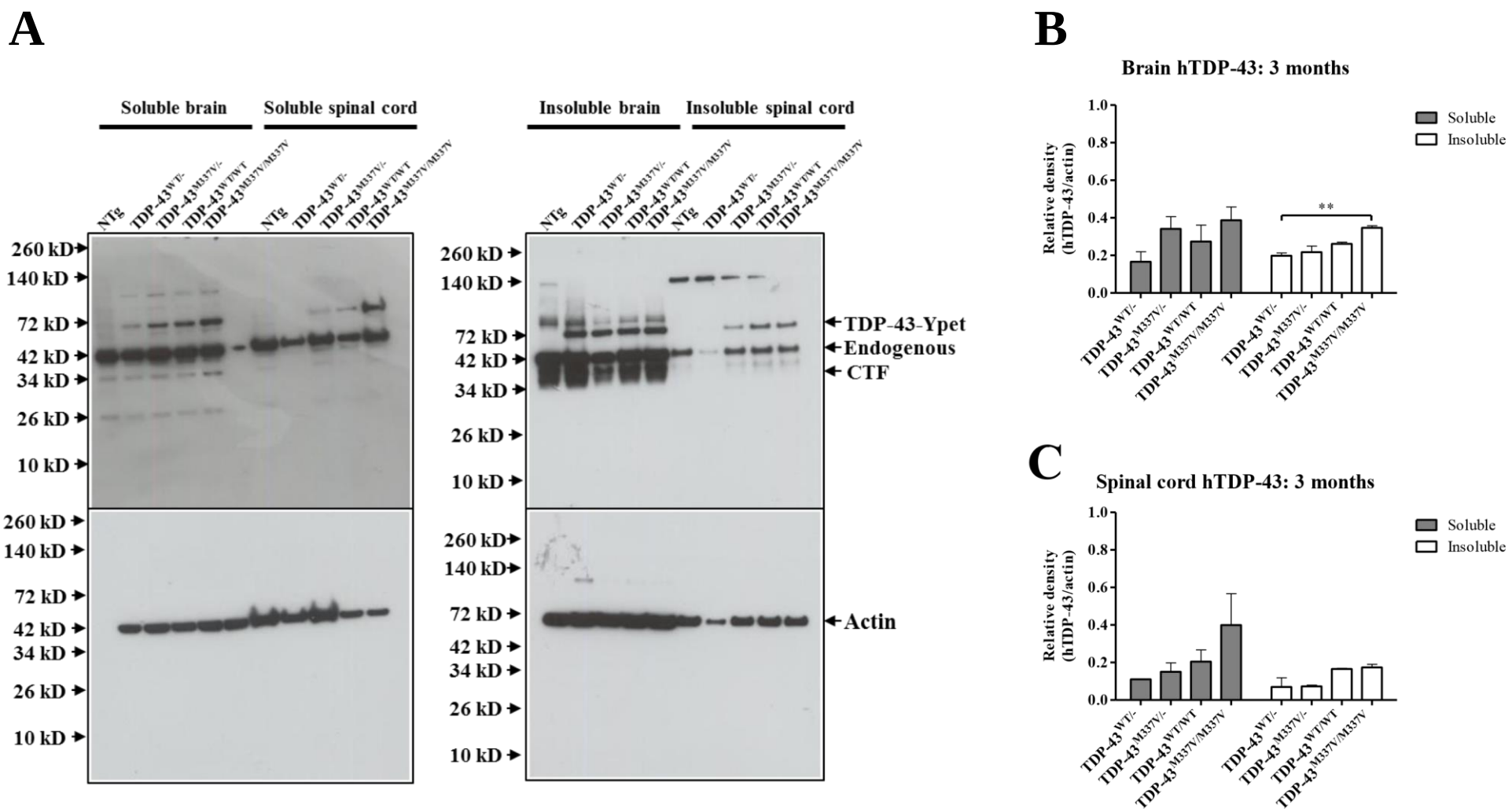
A
Soluble brain
Soluble spinal cord
Insoluble brain
Insoluble spinal cord
NTg
TDP-43WT/-
TDP-43M337V/-
TDP-43WT/WT
TDP-43M337V/M337V
260 kD
140 kD
72 kD
42 kD
34 kD
26 kD
10 kD
TDP-43-Ypet
Endogenous
CTF
Actin
B
Brain hTDP-43: 3 months
Relative density (hTDP-43/actin)
Soluble
Insoluble
**
C
Spinal cord hTDP-43: 3 months

Supp. Fig. 6

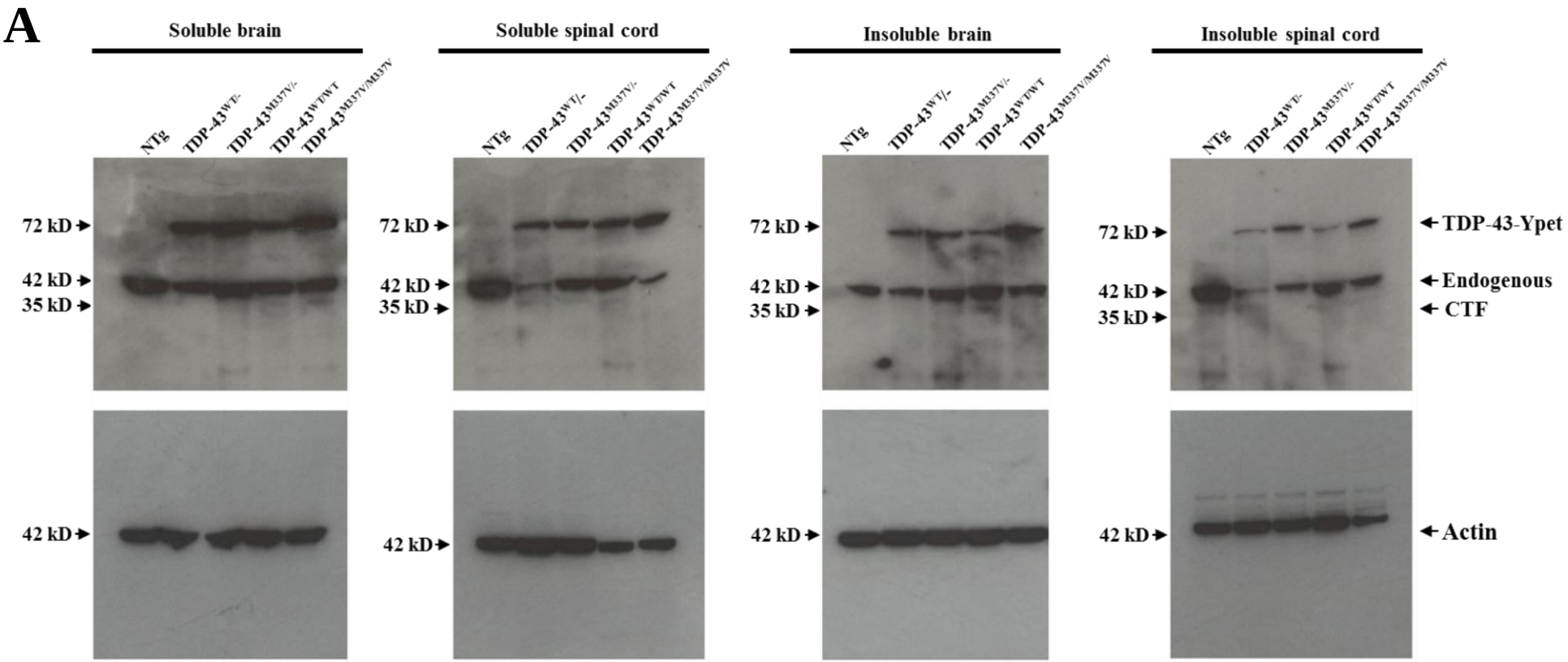

B

Brain hTDP-43: 9 months

C **Spinal cord hTDP-43: 9 months**

Supp. Fig. 7

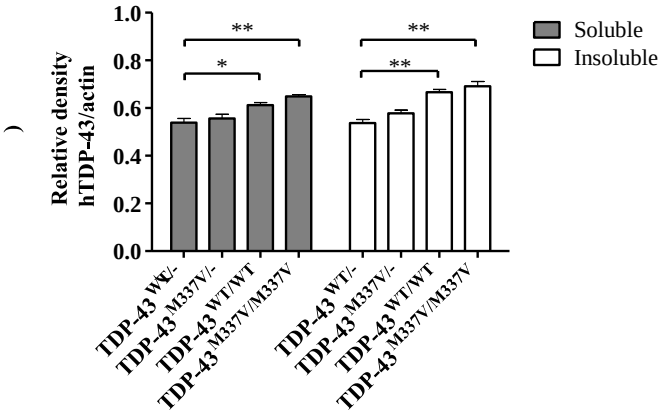
Relative density
hTDP-43/actin
1.0
0.8
0.6
0.4
0.2
0.0
**
*
**
**
Soluble
Insoluble
TDP-43 WT/-
TDP-43 M337V/-
TDP-43 WT/WT
TDP-43 M337V/M337V
TDP-43 WT/-
TDP-43 M337V/-
TDP-43 WT/WT
TDP-43 M337V/M337V

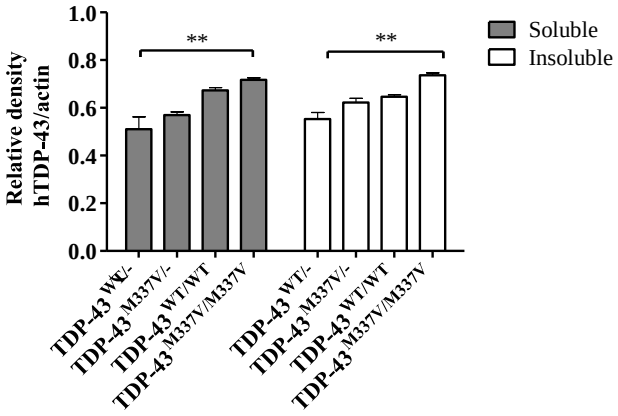
Relative density
hTDP-43/actin
1.0
0.8
0.6
0.4
0.2
0.0
**
**
Soluble
Insoluble
TDP-43 WT/-
TDP-43 M337V/-
TDP-43 WT/WT
TDP-43 M337V/M337V
TDP-43 WT/-
TDP-43 M337V/-
TDP-43 WT/WT
TDP-43 M337V/M337V

A

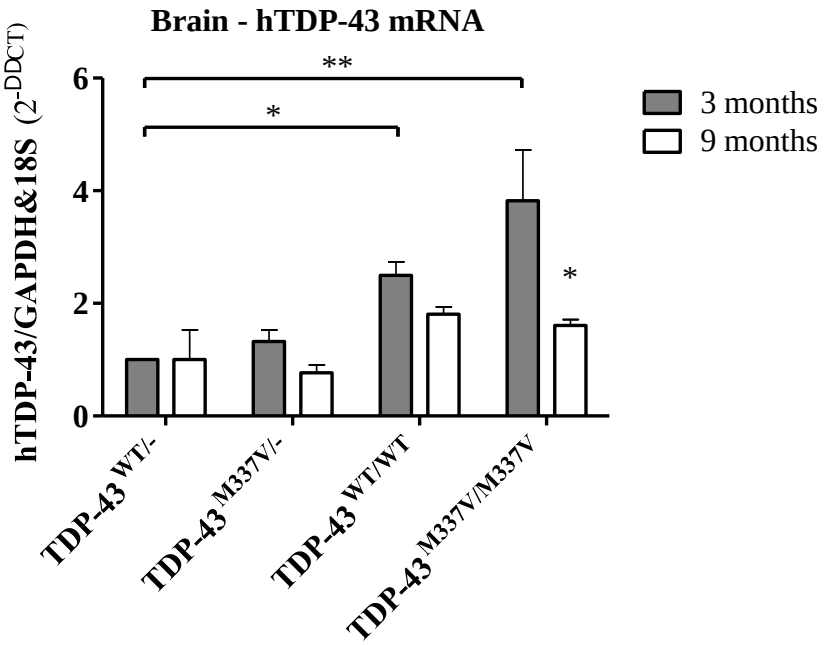
Brain - hTDP-43 mRNA
hTDP-43/GAPDH&18S (2-DDCT)
6
4
2
0
**
*
*
3 months
9 months
TDP-43 WT/-
TDP-43 M337V/-
TDP-43 WT/WT
TDP-43 M337V/M337V

B

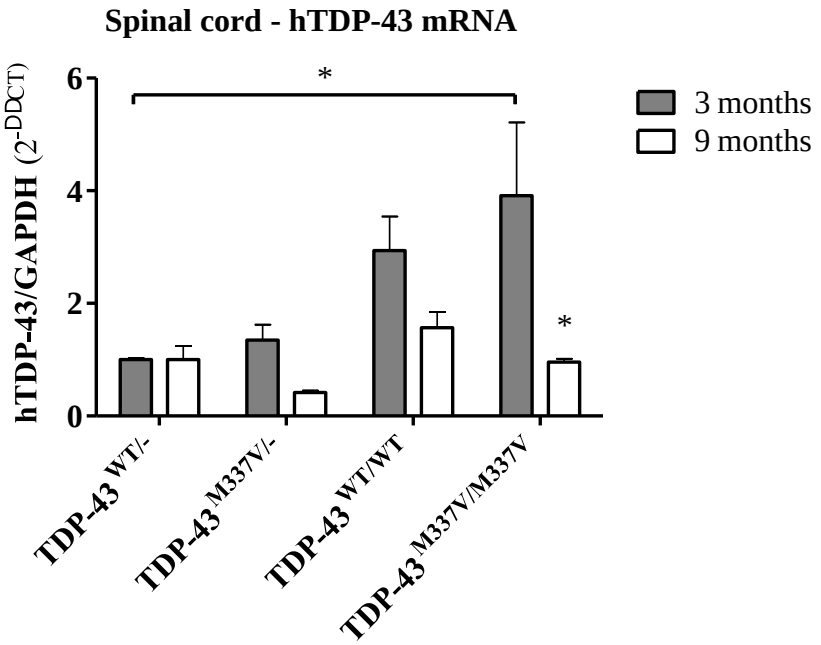
Spinal cord - hTDP-43 mRNA
hTDP-43/GAPDH (2-DDCT)
6
4
2
0
*
*
3 months
9 months
TDP-43 WT/-
TDP-43 M337V/-
TDP-43 WT/WT
TDP-43 M337V/M337V

Supp. Fig. 8

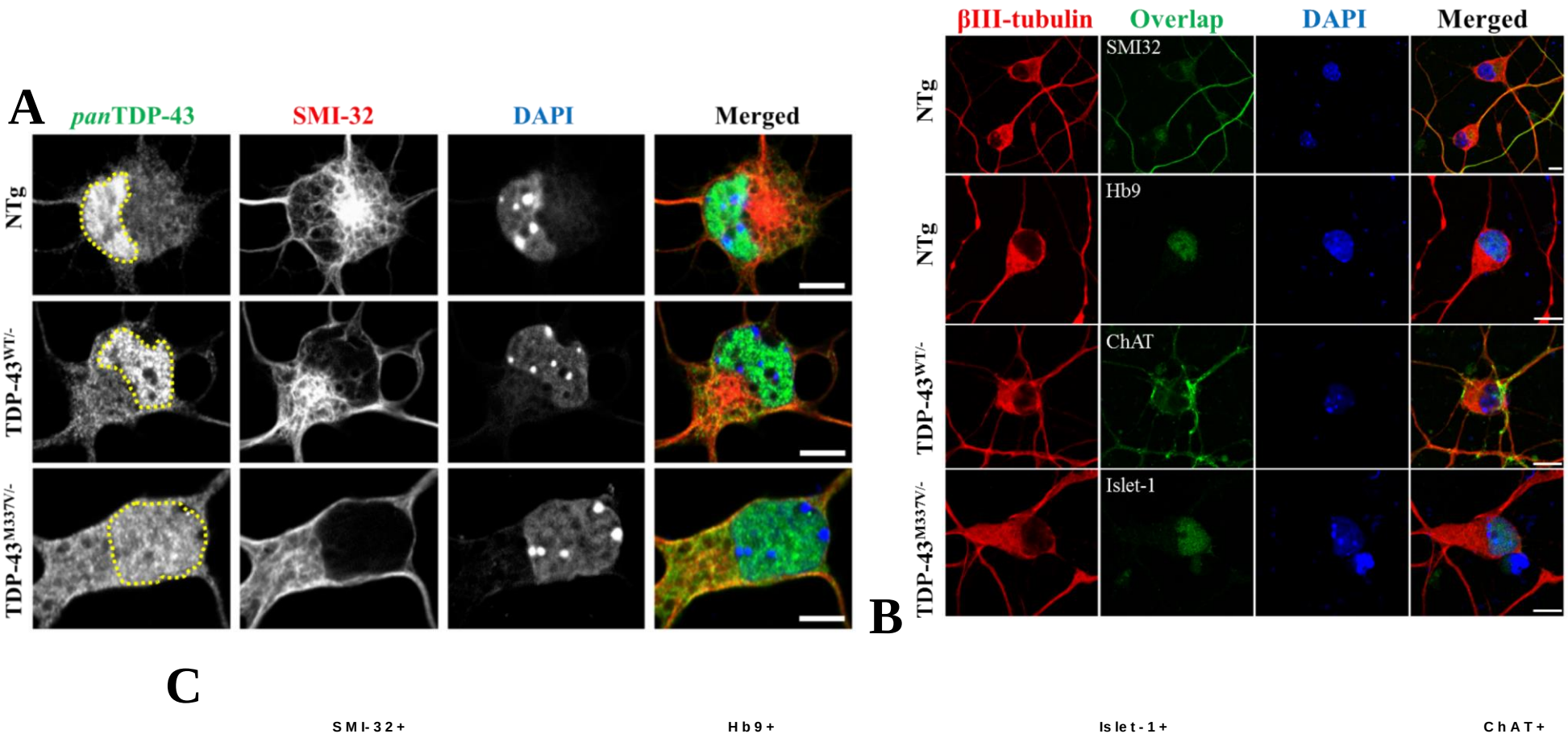
A
panTDP-43
SMI-32
DAPI
Merged
NTg
TDP-43WT/-
TDP-43M337V/-
B
βIII-tubulin
Overlap
DAPI
Merged
SMI32
Hb9
ChAT
Islet-1
C
SMI-32+
Hb9+
Islet-1+
ChAT+

Supp. Fig. 9

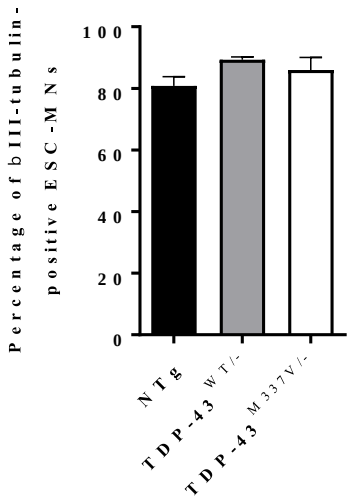

A

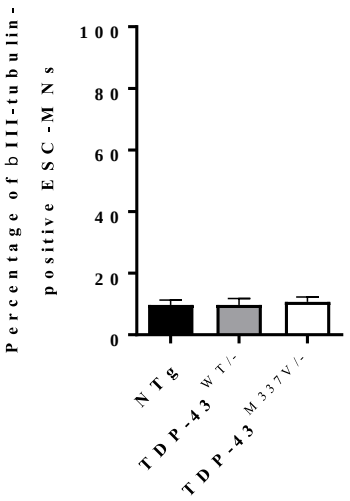

B

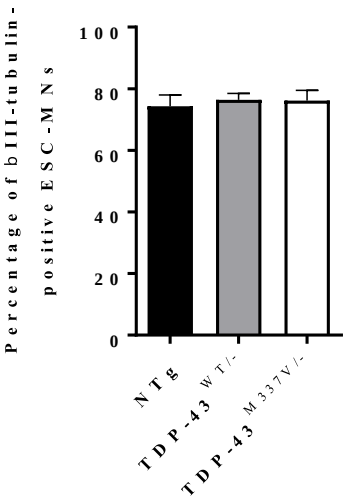

C

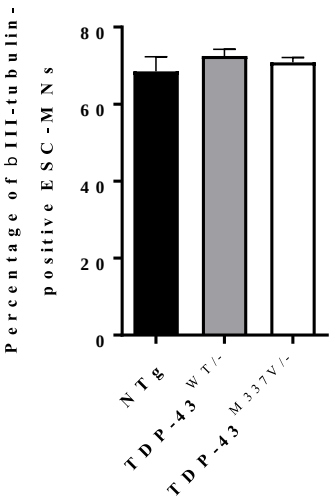

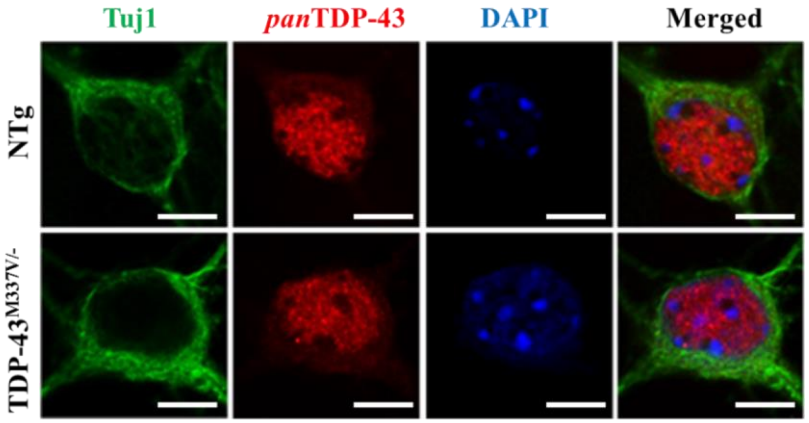

D

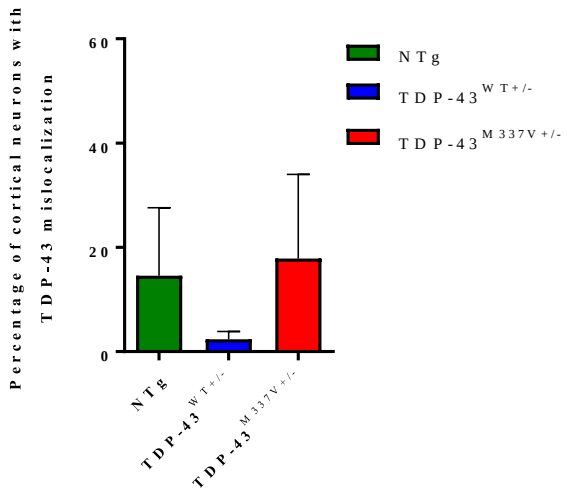

E

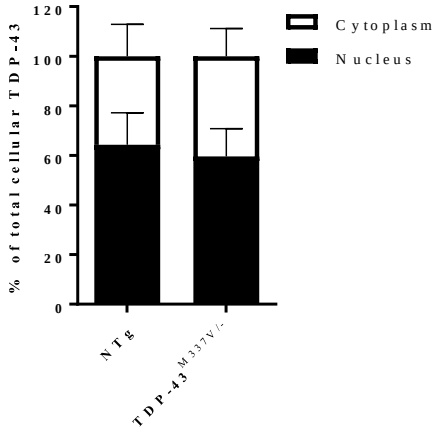

F

Supp. Fig. 10

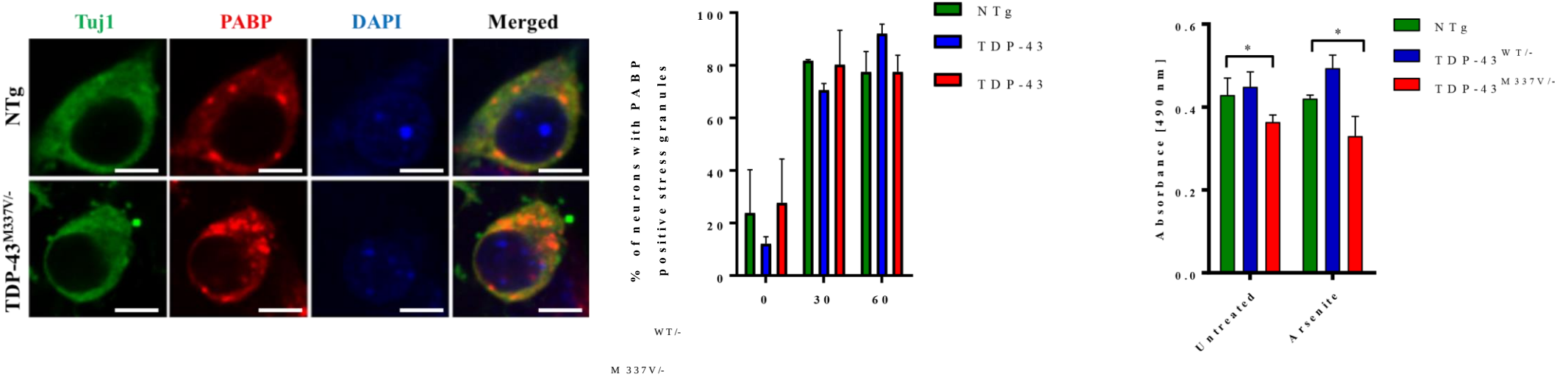

Supplementary Figure 9. Western blots from Figure 1

Fig. 1B – *pan*TDP-43

Supp. Fig. 11

kD Fig. 1B – Actin

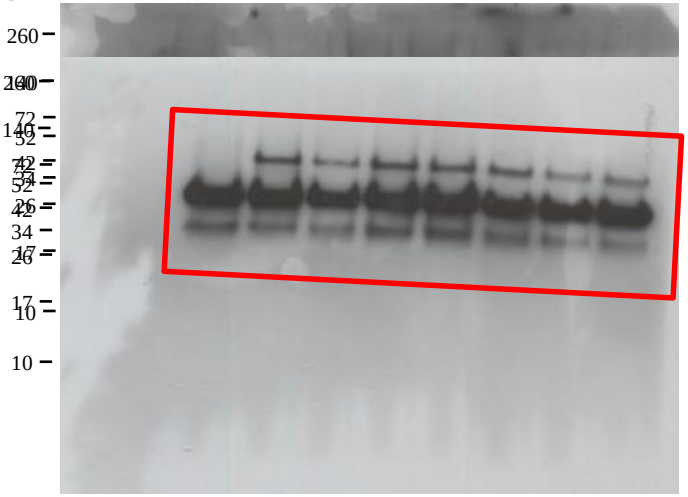

Fig. 1C – *pan*TDP-43

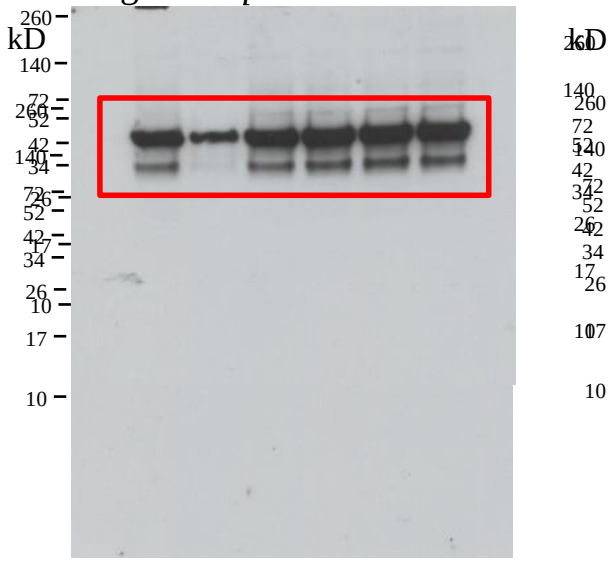

kD Fig. 1C – *pan*TDP-43

Supp. Fig. 12

Fig. 1C – *pan*TDP-43

kD Fig. 1C – Actin

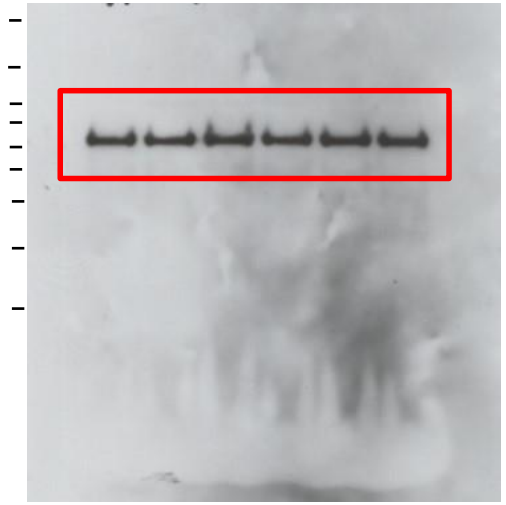

Supp. Fig. 13

Western blots

Supplementary Figure 10. from Figure 1

kD Fig. 1D – *pan*TDP-43

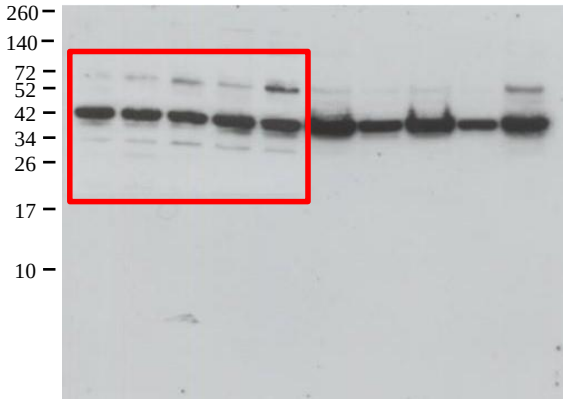

Western blots

Fig. 1D – Actin

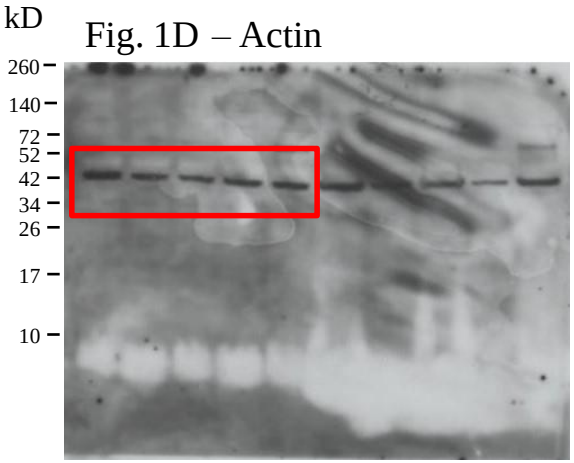

Fig. 1D – *pan*TDP-43

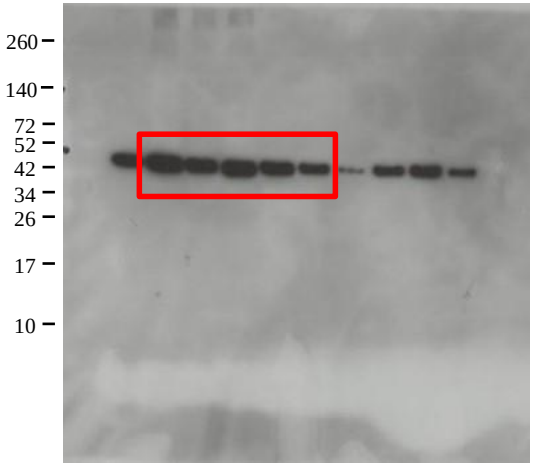

Supp. Fig. 15

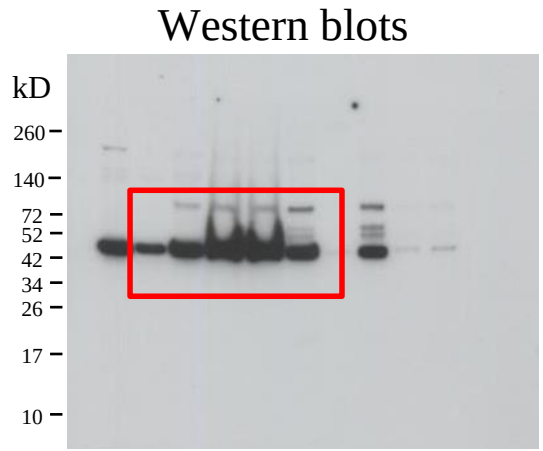

kD Fig. 1D – Actin

Supplementary Figure 11. from Figure 6

Western blots

Fig. 6F – *pan*TDP-43

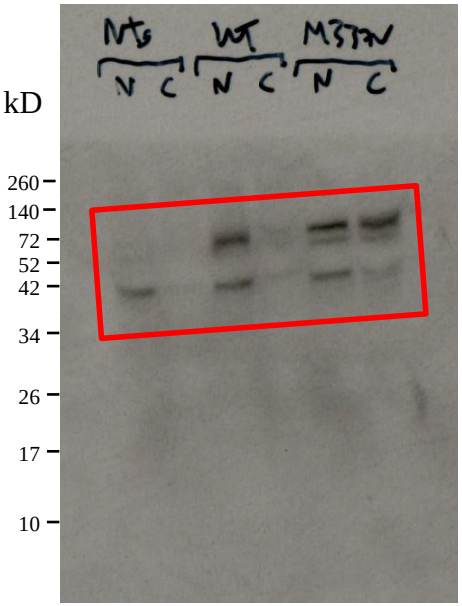

Fig. 6F – Histone H3

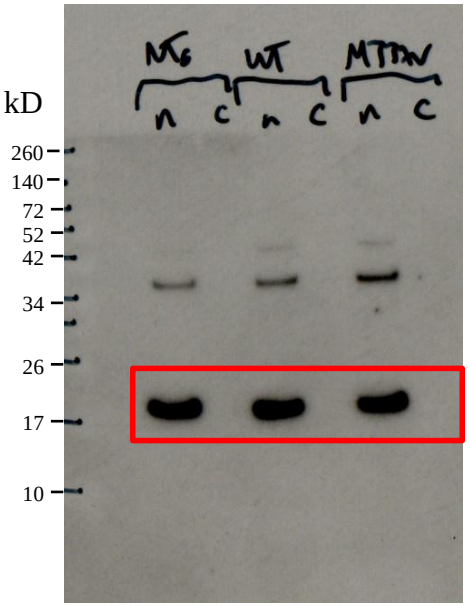

Fig. 6F – GAPDH

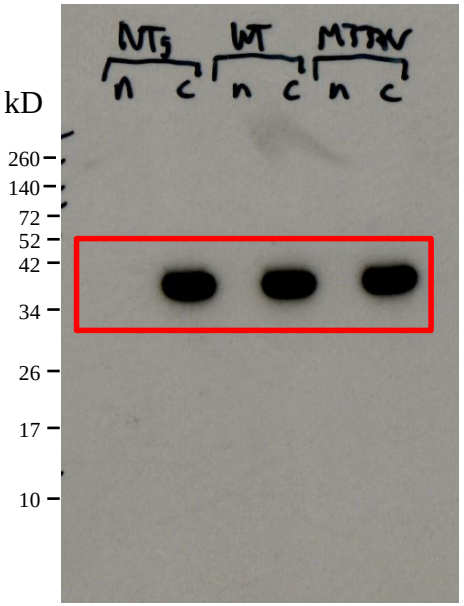

Ponceau stain

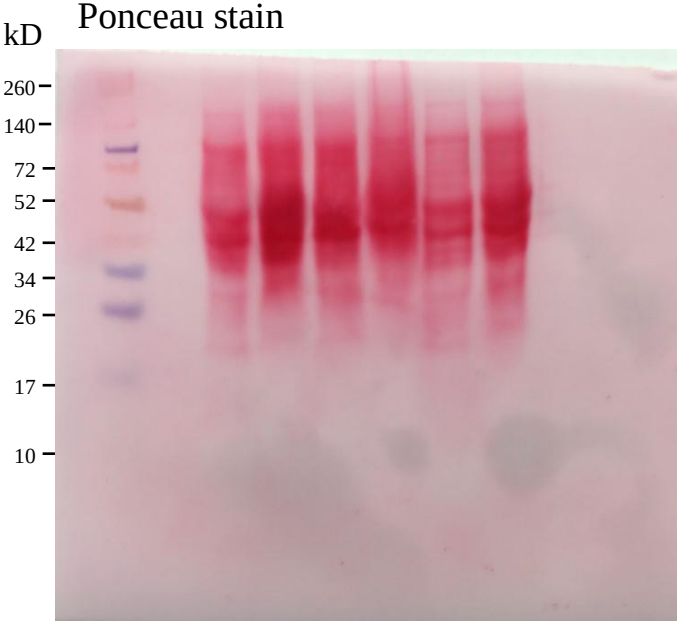

Supplementary Figure 12.

Supp. Fig. 3A – *pan*TDP-43

Western blots

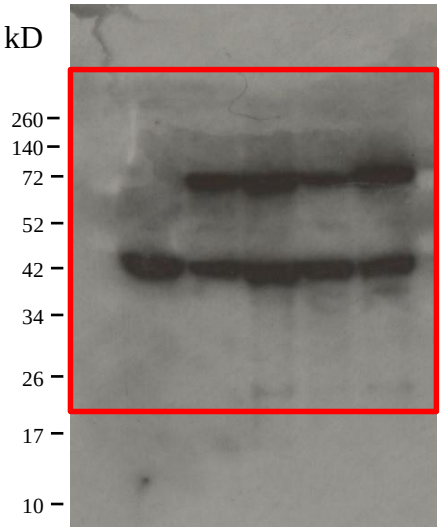

Supp. Fig. 3A – *pan*TDP-43

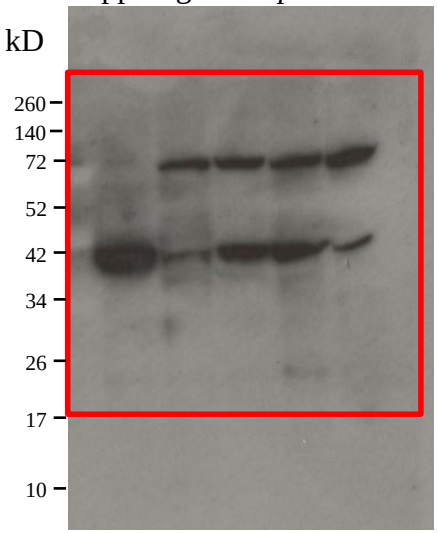

Supp. Fig. 3A – *pan*TDP-43

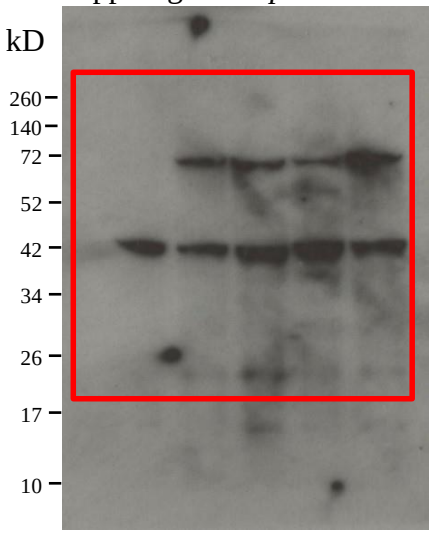

Supp. Fig. 3A – *pan*TDP-43

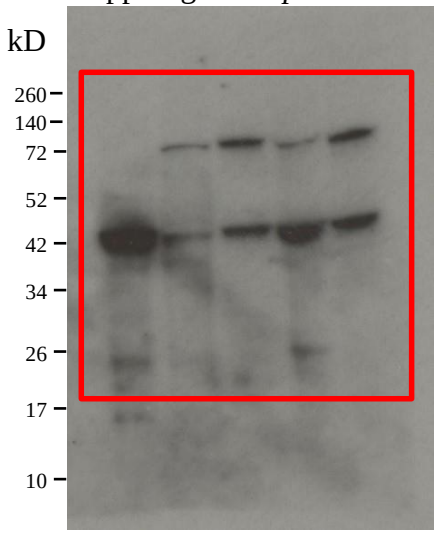

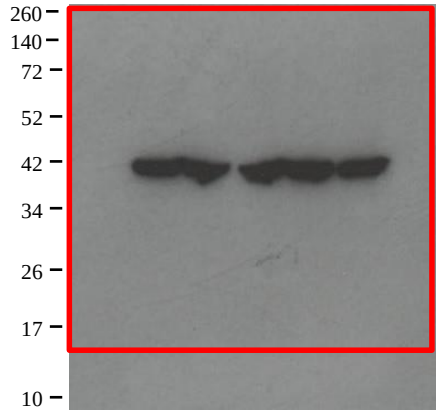

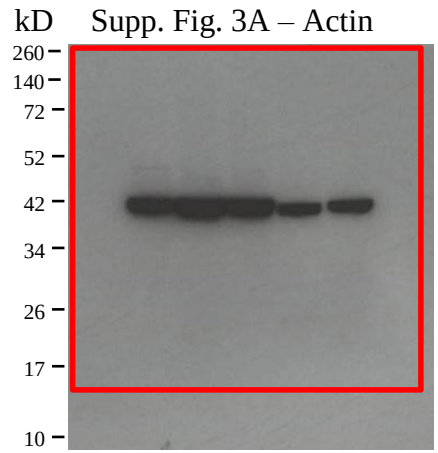

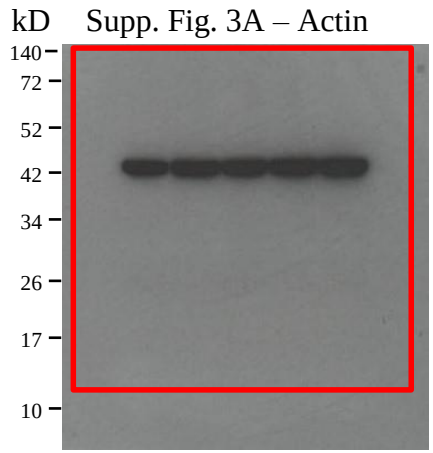

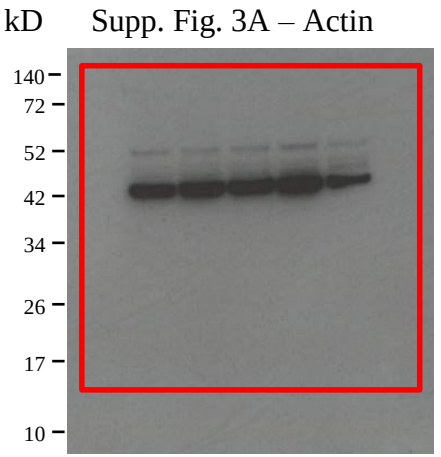

from Supplementary Figure 5